Extended Hückel Study of the Metallic Growth of Small Platinum Clusters: Structure and Energetics

B. Bigot† and C. Minot*‡

Contribution from the Laboratoire de Chimie Organique Théorique,[1] Université Pierre et Marie Curie, 75230 Paris, France, Ecole Normale Supérieure de Saint-Cloud, 92211 Saint-Cloud, France, and Laboratoire de Chimie Théorique,[1] Université de Paris Sud, 91405 Orsay Cedex, France. *Received December 28, 1983*

Abstract: The structure and energetics of small platinum clusters Pt_n (n = 2-13) are studied by extended Hückel techniques (EHT) with and without (SO) spin-orbit coupling. At each step of the metallic growth, a large variety of structures with a common minimal interatomic distance (hard-sphere packing) have been considered in order to determine the most stable isomers. The optimum geometry of some of these structures, for which simple distortions could lead to an energy stabilization, have been computed by using a modified version of the classical EHT set of programs which takes into account the short distance interatomic repulsion. The computations also include some infinite one-dimensional ribbons, two-dimensional sheets, and three-dimensional bulk crystals for comparison with the properties of the clusters. Various analyses have been attempted to rationalize the computed structural and energetical characteristics of the metallic growth. The concept of maximum coordination represents a useful guideline, but a more detailed consideration of the local structures is required to satisfactorily describe the growth. It is observed that the cohesive energy is optimal when the cluster fits within a small sphere. The relative SO contribution to the cohesive energy decreases from 32% to 12% on going from the small aggregates to the metal bulk. This variation results from two opposite factors: the decrease of the electronic d population of the metal atoms and the increase of the geometrical constraints associated with local coordination patterns.

1. Introduction and Scope

The chemistry of metal clusters is a fascinating and blooming area of investigation. It has been the subject of numerous experimental[2] and theoretical studies[3] during the last decade. They have contributed greatly to our understanding of this original class of compounds.

Although, because of their size, clusters are often described as normal inorganic molecules, they can also be considered as small pieces of metal, and present strong analogies with the metal surface concerning reactivity.[2c] Thus, metal clusters are at the frontier between molecular chemistry and solid-state physics, and a part of the interest in this field comes from the hope of gaining new insight into the chemical properties of the metal surfaces used in heterogeneous catalysis.[4]

Initially, clusters refered to the smallest purely metallic particles that are described by geometric shapes rather than by a crystallographic lattice with long-range order. By extension, they also refer to polymetallic complexes with a few metallic atoms surrounded by ligands (molecular clusters). As the ligands provide most of the stability of the clusters, naked clusters are chemically unstable species, and therefore most of the experimental data concern the coordinatively fully (or almost fully) saturated compounds.[5] Numerous crystallographic results give detailed information on their structures.[6] Theoretical studies[7] on this class of clusters have led to useful rules to understand their striking properties.

The study of the purely metallic clusters has been mainly motivated by a desire to understand crystal growth and homogeneous nucleation. Such study is also a prerequisite to the theoretical analysis of their properties of interaction with adsorbates or with a supporting material. Some works deal with the dense packing of spheres[8a] by using pairwise central Lennard-Jones potential calculations.[8b] An EHT approach is the purpose of the present paper. It has been motivated by the recent discovery[9] of unusually small platinum clusters on Na-Y zeolites with an estimated average number of atoms per cluster ranging from two to eight. In a following paper, the more stable clusters described here will be used for studying catalytic hydrogenation.

Platinum clusters with 2-13 atoms have been studied in a systematic way by extended Hückel technique (EHT) with and without the spin-orbit coupling (SO) contribution. SO coupling is known to be significant for the atoms of the sixth row. The

† Université Pierre et Marie Curie and Ecole Normale Supérieure de Saint-Cloud.

‡ Université de Paris Sud.

(1) These laboratories constitute the Equipe de Recherche Associee 549 of the CNRS.

(2) (a) Muetterties, E. L.; Rhodin, T. N.; Band, E.; Bruckner, C. F.; Pretzner, W. R. *Chem. Rev.* **1979**, *79*, 91. (b) Davis, S. C.; Klabunde, K. J. *Chem. Rev.* **1982**, *82*, 153-208. (c) Braunstein, P. *CNRS Image Chim.* **1981**, *47*. (d) Ozin, G. O.; Mitchell, S. A. *Angew. Chem. Int. Ed. Engl.* **1983**, *22*, 674. (e) Delcourt, M. O.; Keghouche, N.; Belloni, J. *Nouv. J. Chim.* **1983**, *7*, 131.

(3) (a) Baetzold, R. C. *J. Chem. Phys.* **1971**, *55*, 4363; *Surf. Sci.* **1975**, *51*, 1. Baetzold, R. C. *Adv. Catal.* **1976**, *25*, 1. Baetzold, R. C.; Mack, R. E. *J. Chem. Phys.* **1975**, *62*, 1513. (b) Itoh, H. *J. Appl. Phys.* **1974**, 497; *J. Appl. Phys.* **1974**, *15*, 2311; *J. Phys. F* **1974**, *4*, 1930. (c) Blyholder, G. *Surf. Sci.* **1974**, *42*, 249. (d) Anderson, A. B. *J. Chem. Phys.* **1976**, *64*, 4046. (e) Lauher, J. W. *J. Am. Chem. Soc.* **1978**, *100*, 5305. (f) Messmer, R. P. *Surf. Sci.* **1981**, *106*, 225. Messmer, R. P.; Tucker, C. W.; Johnson, K. H. *Chem. Phys. Lett.* **1974**, *36*, 423. Messmer, R. P.; Knudson, S. K.; Johnson, K. H.; Diamond, J. B.; Yang, C. Y. Phys. *Rev. B* **1976**, *13*, 1396. (g) Khanna, S. N.; Cyrot-Lackmann, F.; Boudeville, Y.; Rousseau-Voilet, J. *Surf. Sci.* **1981**, *106*, 287. Khanna, S. N.; Bucher, J. P.; Buttet, J.; Cyrot-Lackmann, F. *Surf. Sci.* **1981**, *106*, 200. Bachmann, C.; Demuynck, J.; Veillard, A. 32 reunion Int. Soc. Chim. Physique Villeurbanne, Feb. 11, 1979, "Growth and Properties of Metal Clusters"; Bourdon, J., Ed.; Elsevier: Amsterdam, 1980, p 269; *J. Chem. Phys.* **1981**, *75*, 3443. Takasu, Y.; Bradshaw, A. M. *Chem. Phys. Solids Their Surf.* **1978**, *7*, 56-86 and references therein. (h) Hoare, M. R.; J. McInnes, *Faraday Discuss. Chem. Soc.* **1976**, *61*, 12. (i) J. Friedel Conference Internationale sur les petites particules et amas metalliques, Lyon, 1976, Colloque II *J. Phys. C Suppl.* **1977**, *7*, 1. (j) Minot, C.; Criado-Sancho, M. *Nouv. J. Chim.* **1984**, *8*, 537.

(4) Muetterties, E. L. *Angew. Chem., Int. Ed. Engl.* **1978**, *17*, 545.

(5) Purcell, K. F.; Kotz, J. C. "Inorganic Chemistry"; W. R. Saunders: Philadelphia, 1977. Cotton, F. A.; Wilkinson, G. "Advanced Inorganic Chemistry", 4th ed.; Wiley-Interscience: New York, 1978.

(6) Johnson, B. F. G. "Transition Metal Clusters"; Wiley: New York, 1980. Band, E.; Muetterties, E. L. *Chem. Rev.* **1978**, *78*, 640. Brewer, L. *Science (Washington, D.C.)* **1982**, *161*, 3837.

(7) Hoffmann, R. *Angew. Chem., Int. Ed. Engl.* **1982**, *21*, 711. Hoffmann, R. *Science (Washington, D.C.)* **1981**, *211*, 995. Burdett, J. K. *J. Chem. Soc., Faraday Trans.* **1974**, *70*, 1599. Wade, K. *Chem. Ber.* **1975**, *11*, 177; *Adv. Inorg. Chem. Radiochem.* **1976**, *18*, 1; *J. Chem. Soc., Chem. Commun.* **1971**, 792.

(8) (a) Basley, B. G. *Nature (London)* **1965**, *208*, 674; **1970**, *225*, 1040. (b) Hoare, M. R.; Pal, P. *Nature (London) Phys. Sci.* **1971**, *230*, 1; **1972**, *236*, 35; *J. Cryst. Growth* **1972**, *17*, 77.

(9) Menorval, L. C.; Fraissard, J.; Ito, T. *J. Chem. Soc., Faraday Trans. 1* **1982**, *78*, 403. Ito, T.; Fraissard, J. *J. Chem. Phys.* **1982**, *76* (11), 5225.

0002-7863/84/1506-6601$01.50/0

Table I. H_{ij} Matrix Elements for the d Orbitals of a Single Platinum Atom

	$(x^2-y^2)^+$	z^{2+}	xy^+	xz^+	yz^+	$(x^2-y^2)^-$	z^{2-}	xy^-	xz^-	yz^-
$(x^{2+}-y^2)$	h	0	$-i\xi$	0	0	0	0	0	$1/(2\xi)$	$i/(2\xi)$
z^{2+}	0	h	0	0	0	0	0	0	$-3^{1/2}/(2\xi)$	$i3^{1/2}/(2\xi)$
xy^+	$i\xi$	0	h	0	0	0	0	0	$-i/(2\xi)$	$1/(2\xi)$
xz^+	0	0	0	h	$-i/(2\xi)$	$-1/(2\xi)$	$3^{1/2}/(2\xi)$	$i/(2\xi)$	0	0
xz^+	0	0	0	$i/(2\xi)$	h	$-i/(2\xi)$	$-i3^{1/2}/(2\xi)$	$-1/(2\xi)$	0	0
(x^2-y^2)	0	0	0	$-1/(2\xi)$	$i/(2\xi)$	h	0	$i\xi$	0	0
z^{2-}	0	0	0	$3^{1/2}/(2\xi)$	$i3^{1/2}/(2\xi)$	0	h	0	0	0
xy^-	0	0	0	$-i/2\xi$	$-1/(2\xi)$	$-i\xi$	0	h	0	0
xz^-	$1/(2\xi)$	$-3^{1/2}/(2\xi)$	$i/(2\xi)$	0	0	0	0	0	h	$i/(2\xi)$
yz^-	$-i/(2\xi)$	$-i3^{1/2}/(2\xi)$	$^1/_2\xi$	0	0	0	0	0	$-i/(2\xi)$	h

Table II. Parameters used in EHT Calculations

orbital		H_{ii}, eV	$\exp_1$	$\exp_2$	c_1	c_2
Pt	5d	-12.59	6.013	2.696	0.6334	0.5513
	6s	-10.00	2.554			
	6p	-5.475	2.554			
H	1s	-13.60	1.300			

results without SO coupling allow a molecular analysis with the symmetries and would be suitable for an estimation of the factors governing the stability of nickel and palladium clusters, while those with SO coupling are more realistic as far as platinum is concerned. Some examples of larger clusters (Pt_{14}–Pt_{19}) have also been considered. For comparison with these calculations on small metallic aggregates, various computations have been performed on the bulk metals as well as on infinite metal sheets of different thickness and crystallographic orientation.

2. Calculation Methods

Calculations on the various cluster structures have been performed by using the weighted H_{ij} EHT hamiltonian[10a] with and without the SO coupling contribution. Calculations on infinite structures use extensions of the same programs[10b,11] within the tight-binding scheme.[12] Energies are calculated as the average over a representative number of points in the reciprocal space.[13] The similarity of both calculation techniques allows useful comparison between both types of structures. The consideration of the SO coupling requires that we use as an atomic orbital basis both the α and β spin atomic orbitals. Thus, the EHT + SO hamiltonian matrix is twice as large as the classical EHT matrix. It can be easily shown that the form of the EHT + SO matrix is

$$\begin{bmatrix} M & -N^* \\ N & M^* \end{bmatrix}$$

The associated complex eigenvalue problem can be solved in the quaternion space by the following equation $(M + jN)(u + jv) = \lambda(u + jv)$. It leads to degenerate values for the couple of eigenvectors (u, v) and $(v^*, -u^*)$. The elements of the complex submatrices M and N for a platinum atom are presented on Table I. The EHT parameters are listed on Table II. The parameter ξ of spin–orbit coupling is 0.624 51 eV.[14]

The large number of structures that had to be considered prevented a systematic research of their optimal geometry. Thus, except for mentioned specific cases, every considered structure is built with the same minimum interatomic distance (MID) of 2.77 Å. Such a model corresponds to a hard-sphere packing of platinum atoms. The length of 2.77 Å has been commonly used in previous studies.[10b,15] It is in close agreement with the experimentally determined distance in the bulk metal.[2,16] The hard-sphere assumption sounds a reasonable approximation although it is usually estimated that the metal–metal distance is shorter (approximately 0.1 Å) in small clusters than in the metal bulk.[2] For a few structures, geometrical optimization has been performed with a modified version of the classical EHT program since the classical method is unable to estimate the bond lengths. The present modified version introduces a repulsive part in the interatomic potential. Two ways of introducing this correction have been considered. The first one consists of modifying the Wolfsberg–Helmoltz formula for the interaction between two orbitals. Various authors have proposed different correction formulas.[17a] For the sake of simplicity, we replace the classical hamiltonian H_{ij} by the expression $H_{ij}(1 - \exp(a - bR))$, where R is the interatomic distance, and a and b are parameters. It is imposed that R remains significantly larger than R_o $(=a/b)$ to prevent the new hamiltonian to vanish at short distance while the overlap is large.[18] At large distances, the correction is insignificant, but it increases rapidly with interatomic compression around the MID. The parameters a and b have been adjusted to get an optimal distance of 2.77 Å for the Pt_{13} highly symmetric cuboctahedron structure. Several sets of values satisfy this requirement depending on the value of R_o. Since no clear cut argument allows us to choose among the different possibilities, three sets of parameters have been considered. They correspond to R_o, a, and b equal to 2.5 Å, 39.375, 15.75 Å^{-1}; 2.6 Å, 70.2, 27.0 Å^{-1}; 2.65 Å, 19.25, 45.0 Å^{-1}, respectively. The second way of taking into account the repulsion is to consider that the main neglected factor in the EHT is the nuclear repulsion and to use a two-step calculation by adding an atom–atom repulsive energy to the classical one-electron energy.[17b] The formula $\exp(c - dR)$ has been found to give reasonable results for the corrected EHT.[17c] We select four sets of values for the coupled parameters (c, d) in order to scan different relative magnitudes of the core–core repulsion (see Table VII).

3. Guidelines in the Selection of the Structures

The experimentally determined structures of the molecular clusters depict a wide variety of geometries. Their analysis[2] shows that a large fraction of the polyhedra defined by the purely metallic network have only triangular faces. At the start of the present

(10) (a) Hoffmann, R. *J. Chem. Phys.* **1963**, *39*, 1397. Hoffmann, R.; Lipscomb, W. N. *J. Chem. Phys.* **1962**, *36*, 2179, 3489; **1962**, *37*, 2872. The off-diagonal hamiltonian elements H_{ij} are derived from the diagonal terms by using the modified Wolsberg–Helmoltz formula. Hoffmann, R.; Hofmann, P. *J. Am. Chem. Soc.* **1976**, *98*, 598. (b) Minot, C.; Van Hove, M.; Somorjai, G. *Surf. Sci.* **1982**, *127*, 441.

(11) Whangbo, M.-H.; Hoffmann, R. *J. Am. Chem. Soc.* **1978**, *100*, 6093. Whangbo, M.-H.; Foshee, H. J.; Hoffmann, R. *Inorg. Chem.* **1980**, *19*, 1723.

(12) Andrē, J. M. *J. Chem. Phys.* **1969**, *50*, 1536.

(13) Chadi, D. J.; Cohen, M. L. *Phys. Rev. B* **1973**, *8*, 5747.

(14) Herman, F.; Skillman, F. "Atomic Structure Calculations"; Prentice-Hall: Englewood Cliffs, NJ, 1963; Chapter II.

(15) Baetzold, R. *Chem. Phys.* **1979**, *38*, 313.

(16) "Handbook of Chemistry and Physics", 55th ed.; CRC Press: Cleveland, OH, 1973. Wells, A. F. "Structural Inorganic Chemistry", 3rd ed.; Oxford University Press: London, 1962; Vol. 24.

(17) (a) Engelke, Z.; Beckel, C. L. *Int. J. Quantum Chem.* **1974**, *58*, 209. Guerillot, C. R.; Lissilour, R.; Le Beuze *Theor. Chim. Acta* **1979**, *52*, 1. (b) Gavezzotti, A.; Simonetta, M. *Surf. Sci.* **1980**, *99*, 453. Gavezzotti, A.; Simonetta, M. *Acta Crystallogr., Sect. A* **1975**, *A31*, 645; **1976**, *A32*, 997. Gavezzotti, A.; Simonetta, M.; Van Hove, M.; Somorjai, G. *Surf. Sci.* **1982**, *122*, 292. (c) Anderson, A. *J. Chem. Phys.* **1974**, *60*, 2477. Anderson, A. *J. Chem. Phys.* **1975**, *62*, 1187. Anderson, A.; Hoffmann, R. *J. Chem. Phys.* **1974**, *60*, 4271.

(18) The procedure used to introduce repulsive contributions affects the interaction term H_{ij} without modifying the overlap term S_{ij}. While R tends to R_o, H_{ij} becomes small relative to ES_{ij} leading to artifacts known as the "counterintuitive effect": Whangbo, M.-H., Hoffmann, R. *J. Chem. Phys.* **1978**, *68*, 5498.

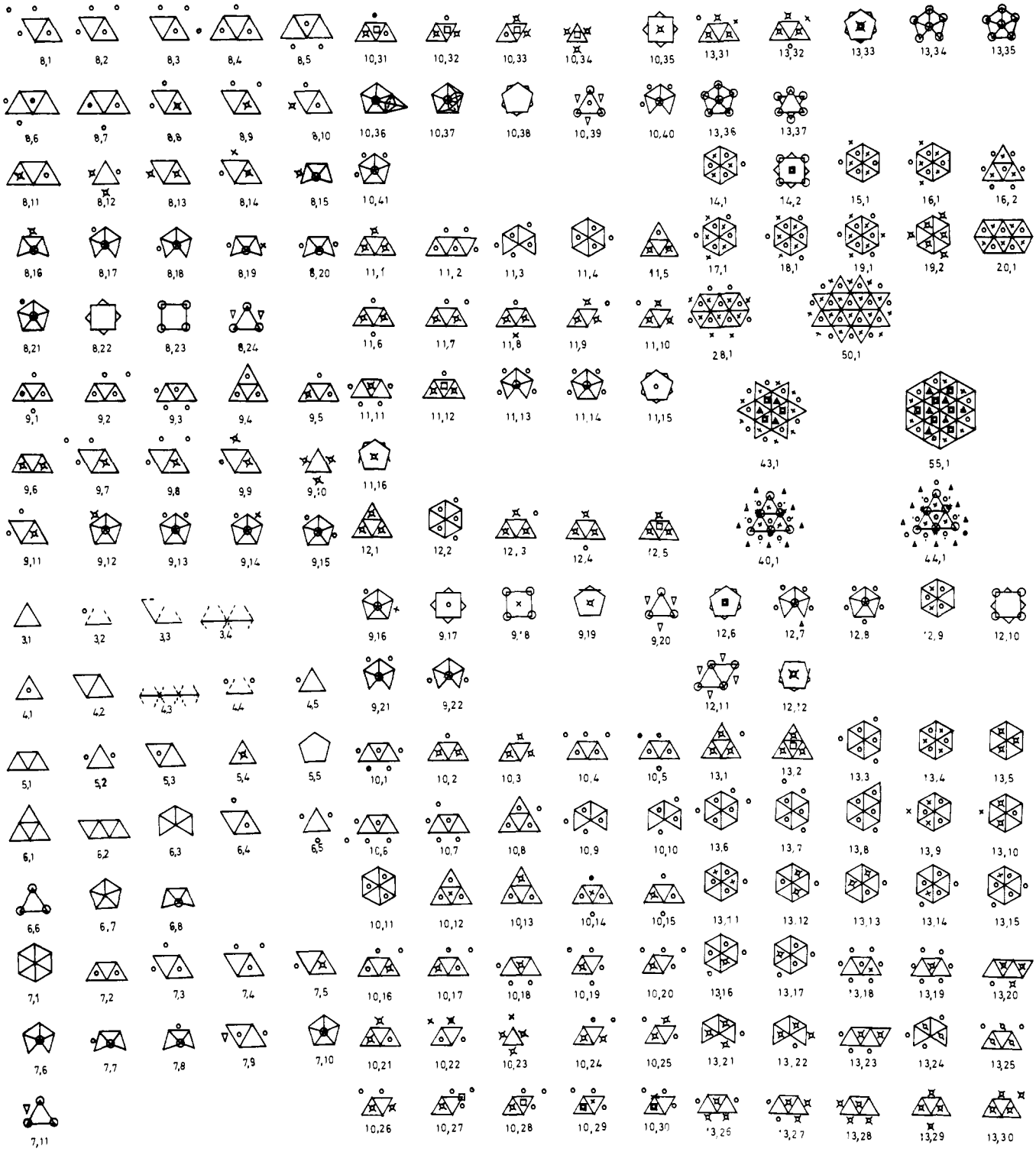

Figure 1. Diagrammatic description of clusters. For the isomers of class A, the full lines depict the nearest-neighbor relationship for atoms located in a reference CPTL plane of bench mark 0. A small circle (○), a cross (×), a small square (□), and a small triangle (△) represent the projection on this plane of atoms located in the CPTL planes +1, −1, +2, and −2, respectively. For the isomers of class B and C, the full lines depict the nearest-neighbor relationship for a simple convex polyhedron, projected along a selected direction. This direction is that of the symmetry axis of higher order, if there is any. A small circle (○) and a cross (×) depict atoms capping the triangular faces of the polyhedron and located above and below the reference plane perpendicular to the selected direction. A small triangle (△) depicts an atom capping a square face of the polyhedron.

study, structures were intentionally chosen without any specific restriction. However, some factors governing the stability of the clusters rapidly emerged; the most obvious is the compactness of the structure. The sphericity of the cluster is a possible approach of the compactness. The corresponding index number would be the radius of the sphere containing the cluster. This compactness index number, however, is not directly related to the number of individual metal–metal interactions as is the number of MIDs which is chemically meaningful. The average number of MIDs per atom is half the average coordination number,[19] if only first-nearest neighbors are considered as coordinating. The largest value, six MIDs per atom, is observed for the fcc packing of the

(19) Desjonqueres, M. C.; Spanjaard, D. *J. Phys. C: Solid State Phys.* **1982**, *15*, 4007; **1983**, *16*, 3389. Thuault-Cytermann, C.; Desjonqueres, M. C.; Spanjaard, D. *J. Phys. C: Solid State Phys.* **1983**, *16*, 5687.

Table III. Calculated Energy Data on Clusters

	nm no. MIDs	EHT	EHT/ nm	EHT + SO	(EHT + SO)/nm	%SO		nm no. MIDs	EHT	EHT/ nm	EHT + SO	(EHT + SO)/nm	%SO
(2,1)	1	0.432	0.43	0.520	0.52	16.9	(10,2)	25	10.8539	0.44	12.7439	0.51	14.8
(3,1)	3	1.164	0.39	1.560	0.52	24.4	(10,3)	25	11.0036	0.44	12.8684	0.51	14.5
(3,2)	2	0.912	0.46	1.119	0.56	18.4	(10,5)	24	10.3638	0.43	12.2660	0.51	15.5
(3,3)	2	0.892	0.45	1.088	0.54	18.0	(10,8)	24	10.2737	0.41	12.207	0.51	15.8
(3,4)	2	0.817	0.41	0.996	0.50	18.0	(10,9)	24	10.6559	0.44	12.6234	0.53	15.6
(4,1)	6	2.4562	0.41	3.5070	0.58	30.0	(10,11)	24	10.6664	0.44	12.4982	0.52	14.7
(4,2)	5	2.0053	0.40	2.8587	0.57	30.0	(10,12)	24	10.3582	0.43	12.2145	0.51	15.2
(4,3)	3	1.2028	0.40	1.4726	0.49	18.0	(10,13)	24	10.3851	0.43	12.2781	0.51	15.4
(4,4)	4	1.7902	0.45	2.3872	0.60	25.0	(10,14)	24	10.4591	0.44	12.2432	0.51	14.6
(4,5)	5	1.9815	0.40	2.9664	0.59	32.0	(10,16)	24	10.3875	0.43	12.3291	0.51	15.7
(5,1)	7	3.0145	0.43	3.9732	0.57	24.0	(10,19)	24	10.3982	0.43	12.3093	0.51	15.5
(5,2)	8	3.7967	0.47	4.9334	0.62	23.0	(10,21)	24	10.5630	0.44	12.4510	0.52	15.2
(5,4)	9	4.0289	0.45	5.2163	0.58	23.0	(10,23)	24	10.6740	0.44	12.7275	0.53	16.1
(5,5)	5	2.3075	0.46	2.9219	0.58	21.0	(10,24)	24	10.5537	0.44	12.4938	0.52	15.5
(6,1)	9	3.8747	0.43	4.9779	0.55	22.0	(10,27)	24	10.5852	0.44	12.5188	0.52	15.5
(6,2)	9	3.8813	0.43	4.9670	0.55	21.0	(10,31)	24	10.3294	0.43	12.2987	0.51	16.0
(6,3)	9	4.1131	0.46	5.1320	0.57	20.0	(10,33)	24	10.2051	0.425	12.1416	0.51	16.0
(6,4)	11	5.1939	0.47	6.4539	0.59	19.0	(10,34)	24	10.6731	0.45	12.8519	0.54	17.0
(6,5)	12	5.6956	0.47	6.9721	0.58	18.0	(10,35)	24	11.1442	0.46	12.8963	0.54	13.6
(6,6)	9	4.7003	0.52	5.9009	0.66	20.0	(10,36)	>25	10.7955	0.43	12.8306	0.51	15.8
(6,7)	10	4.7718	0.48	5.9464	0.59	20.0	(10,37)	9	7.9186		9.6333		17.8
(6,8)	12	5.4181	0.45	6.6994	0.56	19.0	(10,38)	20	10.0001	0.50	11.6949	0.585	14.5
(7,1)	12	5.540	0.46	6.7829	0.56	18.0	(10,39)	24	10.9296	0.46	12.7985	0.53	14.6
(2,2)	14	6.4149	0.46	7.8315	0.56	18.0	(10,40)	24	10.7304	0.45	12.5912	0.53	14.8
(7,3)	15	6.9104	0.46	8.3597	0.56	18.0	(10,41)	>24	10.7877	0.45	12.6459	0.53	14.7
(7,4)	14	6.5126	0.47	7.8602	0.56	17.0	(11,1)	29	12.3385	0.43	14.4639	0.50	15.0
(7,5)	14	6.5206	0.47	7.8704	0.56	17.0	(11,2)	28	12.1186	0.43	14.6269	0.52	17.0
(7,6)	15	6.8322	0.46	8.2342	0.55	17.0	(11,3)	28	12.1443	0.43	14.4673	0.52	16.0
(7,7)	15	6.6487	0.44	8.0598	0.54	17.0	(11,4)	28	12.1673	0.43	14.3019	0.51	15.0
(7,8)	15	6.6686	0.44	8.1061	0.54	17.0	(11,5)	28	11.9171	0.43	14.0815	0.50	15.0
(7,9)	14	6.2592	0.45	7.6223	0.54	18.0	(11,6)	28	11.9797	0.43	14.0815	0.50	15.0
(7,10)	>15	6.9700	0.46	8.3969	0.56	17.0	(11,7)	28	11.9708	0.43	14.1201	0.50	15.0
(7,11)	13	6.5983	0.51	7.8711	0.61	16.0	(11,8)	28	12.0817	0.43	14.2011	0.51	15.0
(7,12)		5.9611		7.3003		18.3	(11,9)	28	12.0683	0.43	14.3165	0.51	16.0
(8,1)	18	8.0058	0.44	9.6874	0.54	17.0	(11,10)	28	12.1292	0.43	14.3184	0.51	15.0
(8,2)	18	8.1515	0.45	9.6778	0.54	16.0	(11,11)	28	12.1090	0.43	14.3674	0.51	16.0
(8,3)	17	7.862	0.46	9.3600	0.55	16.0	(11,12)	28	11.8844	0.42	14.1882)	0.51	16.0
(8,4)	18	8.0394	0.45	9.6429	0.54	16.0	(11,13)	27	11.9986	0.44	14.1221	0.52	17.7
(8,5)	17	7.8621	0.46	9.356	0.55	16.0	(11,14)	>27	12.0070	0.44	14.1003	0.52	17.4
(8,6)	17	7.8403	0.46	9.3554	0.55	16.0	(11,15)	25	11.9587	0.48	13.7980	0.55	15.3
(8,7)	17	7.7266	0.45	9.2206	0.54	16.0	(11,16)	10	8.6955		10.5455		17.5
(8,8)	18	8.1891	0.46	9.6996	0.54	16.0	(12,1)	33	13.6330	0.41	16.0689	0.49	15.2
(8,9)	17	7.7418	0.46	9.2504	0.54	16.0	(12,2)	32	13.6284	0.43	16.2178	0.51	16.0
(8,10)	17	7.9322	0.47	9.3525	0.55	15.0	(12,3)	32	13.4442	0.42	15.9454	0.50	15.7
(8,11)	17	7.7260	0.45	9.2747	0.55	17.0	(12,4)	32	13.5030	0.42	15.9019	0.50	15.1
(8,12)	17	8.0412	0.47	9.4827	0.56	15.0	(12.5)	32	13.3514	0.42	16.0488	0.50	16.8
(8,13)	17	7.8931	0.46	9.3842	0.55	16.0	(12,6)	30	13.8892	0.46	15.8689	0.53	12.7
(8,14)	17	7.8718	0.46	9.3256	0.55	15.6	(12,7)	30	13.2767	0.44	15.6304	0.52	17.7
(8.15)	18	7.8496	0.44	9.4587	0.53	17.0	(12,8)	30	13.3010	0.44	15.5928	0.52	10.9
(8,16)	18	8.0416	0.45	9.5942	0.53	16.0	(12,9)	31	13.4717	0.45	15.6986	0.52	16.5
(8,17)	18	8.0497	0.45	9.5970	0.53	16.0	(12,10)	28	13.2359	0.47	15.5106	0.55	14.6
(8,18)	18	7.8146	0.43	9.469	0.53	17.5	(12,11)	30	13.5797	0.45	16.0407	0.53	15.3
(8,19)	18	7.9610	0.44	9.4729	0.53	16.0	(12,12)	11	9.7902		11.8306		17.3
(8,20)	18	7.8829	0.44	9.3964	0.52	16.0	(13,1)	36	14.8028	0.41	17.5627	0.49	15.7
(8,21)	>18	8.1950	0.46	9.7503	0.54	16.0	(13,2)	36	14.6377	0.41	17.6710	0.49	17.0
(8,22)	16	8.1500	0.51	9.4851	0.59	14.0	(13,3)	36	15.0853	0.42	18.1440	0.50	17.0
(8,23)	12	6.8509	0.57	8.2429	0.69	17.0	(13,4)	36	15.3316	0.43	17.7659	0.49	14.0
(8,24)	17	8.2702	0.49	9.6999	0.57	14.7	(13,5)	36	15.3470	0.43	17.7199	0.49	13.0
(8,25)		7.0335		8.4686		16.9	(13,8)	35	14.7986	0.42	17.7465	0.51	16.6
(9,1)	21	9.2738	0.44	10.9744	0.52	15.5	(13,14)	35	14.803	0.42	17.6174	0.50	16.0
(9,2)	21	9.1838	0.44	10.9635	0.52	16.0	(13,18)	35	14.7614	0.41	17.5863	0.49	16.0
(9,3)	21	9.4429	0.45	11.1484	0.53	15.0	(13,19)	35	14.6697	0.42	17.5195	0.50	16.3
(9,4)	21	9.0738	0.43	10.8633	0.52	16.5	(13,21)	35	14.9353	0.43	17.6896	0.505	15.6
(9,5)	21	9.3090	0.44	11.0160	0.52	15.5	(13,23)	35	14.9713	0.43	17.8604	0.51	16.2
(9,6)	21	9.3416	0.44	11.0753	0.52	15.6	(13,25)	35	14.4803	0.41	17.3481	0.50	16.5
(9,7)	21	9.3047	0.44	11.0689	0.53	15.9	(13,29)	35	14.6257	0.42	17.3175	0.50	15.5
(9,8)	21	9.3074	0.44	11.0012	0.52	15.4	(13,30)	35	14.5438	0.42	17.3548	0.50	16.2
(9,9)	21	9.4724	0.45	11.1238	0.53	14.8	(13,33)	12	13.7875		16.0833		14.2
(9,10)	21	9.5988	0.46	11.2431	0.53	14.6	(13,34)	35	14.9688	0.43	17.5903	0.50	14.9
(9,11)	21	9.2575	0.44	11.0375	0.53	16.1	(13,35)	30	14.6776	0.49	17.478	0.58	16.0
(9,12)	>21	9.3858	0.45	11.0914	0.53	15.3	(13,36)	20	14.8761		17.5134		15.0
(9,13′)	>>21	9.5105	0.45	11.2040	0.53	18.8	(13,37)	33	15.035	0.45	17.6164	0.53	14.6
(9,14)	>21	9.3652	0.45	11.0304	0.525	15.1	(14,1)	40	16.7992	0.42	19.7304	0.49	14.9
(9,15)	>21	9.4514	0.45	11.1187	0.53	15.0	(14,2)	36	16.6744	0.46	19.3196	0.54	13.7
(9,16)	>21	9.3256	0.44	11.1114	0.53	16.0	(15,1)	44	18.2273	0.41	21.5580	0.59	15.5
(9,17)	20	9.6504	0.48	11.2028	0.56	13.8	(16,1)	48	19.6206	0.41	23.3886	0.49	16.1

Table III (Continued)

	nm no. MIDs	EHT	EHT/ nm	EHT + SO	(EHT + SO)/nm	%SO		nm no. MIDs	EHT	EHT/ nm	EHT + SO	(EHT + SO)/nm	%SO
(9,18)	8	7.5306	0.94	9.4374	1.18	20.0	(16,2)	48	19.3776	0.40	23.4364	0.49	17.3
(9,19)	8	7.1490	0.97	8.7208	1.09	18.0	(17,1)	52	21.1846	0.41	25.3252	0.49	16.4
(9,20)	21	9.8003	0.47	11.4648	0.55	14.5	(18,1)	56	22.9475	0.41	27.2200	0.49	15.7
(9,21)	21	9.3970	0.44	11.0893	0.53	15.2	(19,1)	60	24.3504	0.41	29.0034	0.48	16.0
(9,22)	21	9.3082	0.44	10.9896	0.52	15.3	(19,2)	60	24.2362	0.40	29.0407	0.48	16.5
(9,23)	18	9.2059	0.51	10.6999	0.59	13.4	(19,3)	60	24.3526	0.41	29.0249	0.48	16.1
(10,1)	25	10.9788	0.44	13.0488	0.52	15.9							

Table IV. Fermi Levels for the Various Clusters and the Infinite Systems

	no. MIDs per atom	Fermi level EHT	Fermi level EHT + SO	"s-3p" density EHT
(2,1)	0.5	−11.996	−11.775	0.12
(3,1)	1.0	−11.994	−11.687	0.23
(4,1)	1.5	−11.994	−11.647	0.67
(5,4)	1.8	−11.934	−11.502	0.61
(6,5)	2.0	−11.949	−11.455	0.61
(7,10)	>2.0	−11.888	−11.419	0.58
(8,21)	>2.25	−11.861	−11.394	0.57
(9,20)	2.33	−11.855	−11.441	0.59
(10,1)	2.50	−11.761	−11.306	0.60
(11,1)	2.63	−11.694	−11.306	0.57
(11,2)	2.55	−11.754	−11.381	0.62
(12,2)	2.67	−11.708	−11.306	0.60
(13,3)	2.77	−11.674	−11.299	0.63
(14,1)	2.86	−11.689	−11.282	0.62
(15,1)	2.93	−11.652	−11.247	0.63
(16,1)	3.00	−11.633	−11.225	0.64
(16,2)	3.00	−11.633	−11.302	0.63
(17,1)	3.06	−11.621	−11.257	0.69
(18,1)	3.11	−11.606	−11.296	0.73
(19,1)	3.16	−11.708	−11.285	0.78
(19,2)	3.16	−11.628	−11.312	0.77
(19,3)	3.16	−11.592	−11.282	0.77
chain Pt_6	3.00	−11.646	−11.239	
chain Pt_4	3.25	−11.549	−10.824	
(100) plane				
1 layer	2.00	−11.860	−11.492	0.62
2 layers	4.00	−11.553	−11.174	0.79
3 layers	4.67	−11.408	−11.048	0.88
(111) plane				
1 layer	3.00	−11.828	−11.476	0.83
2 layers	4.50	−11.421	−11.087	0.84
3 fcc layers	5.00	−11.276	−11.010	0.94
3 hcp layers	5.00	−11.308	−11.020	0.91
4 fcc layers	5.25	−11.241	−10.978	0.91
4 hcp layers	5.25	−11.269	−10.991	0.92
4 mix layers	5.25	−11.237	−11.004	0.91
5 fcc layers	5.40	−11.256	−10.997	0.91
5 hcp layers	5.40	−11.244	−10.916	0.91
6 fcc layers	5.50	−11.266	−10.954	0.90
7 fcc layers	5.57	−11.230	−10.923	0.93
9 fcc layers	5.67	−11.216	−10.940	0.94
fcc bulk	6.00	−11.199	−10.842	0.95
hcp bulk	6.00	−11.196	−10.824	0.95

metal bulk. In this packing, the most compact crystallographic plane is the close-packed triangular lattice (CPTL) with an average of three MIDs per atom. A systematic way to generate compact clusters is to stack parts of those planes in a parallel way. Since this plane exists as well in the fcc packing (111) as in the hcp packing (100), structures corresponding to fcc or hcp growth as well as mixed stacked structures will be generated. These structures define an ensemble which we call class A. The distinction between fcc and hcp structures starts with the introduction of the third CPTL parallel plane. The mixed stackings start with the fourth CPTL.

Another way to analyze the fcc and hcp stacks is to consider them as assemblies of elementary volumes. Indeed, the total volume of the fcc or hcp bulk breaks up into two primitive volumes: the tetrahedron T_d with six MIDs for four atoms and the square pyramid P_4 with eight MIDs for five atoms. These primitive volumes can fit into structures that do not pertain to class A. They define the class B. Polytetrahedra are members of this class. Compounds of class B differ from those of class A because they do not constitute a cell suitable to fill (by repetition) the whole space.

Some polytetrahedra are quite remarkable. One is the Pt_7 system with four adjacent tetrahedra that have two atoms in common. This structure is highly compact because the volume built from the four tetrahedra contains a hole into which nearly fits the volume of an extra tetrahedron. The equatorial platinum ring is a distorted pentagon with one side 1.257 times longer than the others. A small elongation of the common edge (by a factor of 1.05) leads to the regular pentagonal bipyramid. Other noticeable polytetrahedra are the Pt_{13} systems with 10 adjacent tetrahedra having one atom in common. These structures may be distorted, yielding an icosahedron that is composed of 20 nonregular tetrahedra with a common atom. This distortion requires an elongation of the external bond lengths by a factor

of 1.05 as for the Pt_7 structure.

These examples show that a third class, named class C, has to be defined. It gathers compact structures involving some elementary volumes other than T_d and P_4. We select these structures on symmetry considerations. These volumes are the pentagonal pyramid P_5, the trigonal prism (10 and 9 MIDs, respectively, for six atoms), the pentagonal antiprism (20 MIDs for 10 atoms), and the icosahedra with 12 or with 13 atoms.

The consideration of structures of class B and C allows exploration of some ways of nucleation different than the normal fcc or hcp metallic growth.

In the next section, the various calculated clusters Pt_n will be presented according to the value of n (n = 2–13, 14–∞). The above classification (A, B, C) will be used. Results involve both the simple EHT and the EHT + SO methods.

4. Comparison of the Pt_n Isomers

In the first part of this section, the value of the MID has been fixed to 2.77 Å. Variations of the MIDs will be examined later for a few isomers. The selected compounds for this optimization are those for which a small difference exists between the first-nearest-neighbor distance (the 2.77-Å MID) and the smallest second-nearest-neighbor distance. All structures are shown in Figure 1.

Pt_1. It is established that the most stable spectroscopic state of the Pt atom is the $3D^3$ state ($(5d)^9(6s)^1$). It is quasi-degenerate with the $3F^4$ state ($(5d)^8(6s)^2$) (+0.1 eV). Next, the $1S^0$ (d^{10}) state comes (+0.76 eV above the $3D^3$ state). The EHT technique is inadequate to reproduce these features: the usual parameters place the 6s atomic orbital at 2.59 eV above the 5d level, whatever the electronic configuration may be. Then, in the following discussions, the d^{10} configuration will be considered as the reference state, even if it is clear that it is not a correct description of the isolated atom.

Spin–orbit coupling splits the energetically degenerate d spin orbitals of the platinum atom (−12.59 eV) into two subsets of four spin orbitals at −13.53 eV and of six spin orbitals at −11.97 eV associated with $J = {}^5/_2$ and $J = {}^3/_2$, respectively. However, the SO interaction has no effect on the total energy since, for a d^{10} configuration, the mean values of the operators $\hat{L}^2$, $\hat{S}^2$, and $\hat{L}\hat{S}$ are equal to zero. Due to the generation of a stabilized set of four spin orbitals for the atom, the influence of the spin–orbit coupling is maximum for a d^4 configuration (such as the hafnium atom) while it is zero for a d^{10} configuration, such as the neutral platinum atom. Following this simple analysis when atoms interact to form clusters, the influence of the spin–orbit coupling enhances the cohesive energy of the Pt_n structures while it reduces that of the Hf_n structures. For the platinum systems, the stabilization due to SO coupling increases with the depopulation of the d set of orbitals and the subsequent population of the s–p set.

Pt_2. The EHT description of Pt_2 induces a mixing between s, p, and d atomic orbitals. The results can be considered as a symmetrical electronic transfer from the d orbitals of one atom to the (s, p) orbitals of the other. It is equivalent to a polarization effect on each center.[20] This effect corresponds to a formal $d(10 - x)\,sp(x)$ atomic configuration with x = 0.12 (Table IV). It is worth noting that the depopulation of the d orbitals affects mainly their in-phase combinations (because of their mixing with the in-phase s MO of low energy) and leads subsequently to a partly occupied d system with an antibonding character. The bonding character between the two atoms is assumed mainly by the in-phase overlap between the s–p orbitals of one atom with the d orbitals of the other. Indeed, the total overlap population matrix (0.156) splits into a major sp–d in-phase contribution (0.171) corrected by a minor out-of-phase d–d term (−0.016). the influence of the sp–sp overlap population is negligible (0.001).

An energy lowering of 0.43 eV results from these interactions at the simple EHT level (Table III). As the atoms no longer have a d^{10} configuration, the spin–orbit coupling induces an extra stabilization of 0.088 eV. It represents 17% of the total stabilization energy.

Pt_3. The class A of the Pt_3 clusters has one structure with three MIDs, the equilateral triangle (3,1), and three structures with two MIDs, the 90° and 120° triangles (3,2) and (3,3) respectively, and the linear structure (3,4). These three structures can be considered as resulting from a continuous distortion of one bond of the structure (3,1).

As in Pt_2, the bonds come from the sp–d interaction between two centers. Since the overlap decreases rapidly with the distance, the structure (3,1) with the largest number of MIDs is the most stable (Table III). The total stabilization energy, compared with 3Pt, is 1.56 eV. The mean cohesive energies per MID are in the range of those observed for Pt_2 (0.52 eV), although (3,2) has a slightly larger value (0.56 eV). This result shows that, to a first approximation, the number of MIDs can be a useful guide to foresee the total cohesive energy of a new cluster. The overlap population per atom of (3,1) is 0.150. It is close to the value found for Pt_2 (0.156) and is similarly split into an sp–d dominant in-phase contribution (0.154) and smaller out-of-phase d–d (−0.018) and in-phase sp–sp (0.014) terms. The action of the spin–orbit coupling induces an extra stabilization energy of 0.40 eV (25% of the total bonding energy) for (3,1). This larger percentage for Pt_3 than for Pt_2 is associated with the increase in the "sp" population (see Table IV). The lengthening of a Pt–Pt distance in going from (3,1) to (3,4) is associated with a regular decrease of the cohesive energies (from 1.16 to 0.82 eV at the simple EHT level and from 1.56 to 1.00 eV at the EHT + SO level).

Pt_4. The structures of Pt_4 of class A and built from the matching of two parallel CPTLs are the tetrahedron (4,1) with six MIDs (the largest number of MIDs of the Pt_4 series), the folded rhombus (4,5), and the square (4,4) with five and four MIDs, respectively. The structures of class A derived from a unique CPTL include the planar rhombus (4,2) with five MIDs and the linear chain (4,3) with three MIDs. As in the Pt_3 series, the order of stability of the various calculated clusters corresponds to the increasing order of the number of MIDs (Table III); the most compact tetrahedron structure (4,1) comes first then (4,5), (4,2), (4,4), and (4,3). Except for (4,3) which has a value similar to the linear structure (3,4), the mean cohesive energy per MID is roughly a constant within the Pt_4 series as in the Pt_2–Pt_3 ensemble. This mean value increases slightly (from 0.52 to 0.58 eV) from the first series to the present one. In the Pt_4 series, a detailed analysis of the EHT results reveals, despite the uniform cohesive energy per MIDs, a discontinuity in the overlap populations: structures (4,1) and (4,5) exhibit large mean values (0.251 and 0.225, respectively) whereas the square (4,4) has a value (0.169) close to the ones found in the series Pt_2 and Pt_3. The value of (4,4) comes from the usual dominant sp–d out-of-phase term (0.164) corrected by the smaller sp–sp in-phase (0.018) and d–d out-of-phase (−0.013) terms. The values for (4,1) and (4,5) split a completely different way. Indeed, there is a large sp–sp in-phase contribution (0.126 and 0.115, respectively), a reduced sp–d in-phase term (0.106 and 0.100, respectively), and a small, but now in-phase, d–d contribution (0.019 and 0.010, respectively). A noticeable discontinuity in the sp electronic density corresponds to this discontinuity in the overlap population. The value for the square (4,4) is small (0.266) and close to the Pt_3 value (0.228) while for the tetrahedron (4,1) and the folded rhombus (4,5), it rises up to 0.666 and 0.649, respectively. The continuity in the energetics and the discontinuity in the overlap population can be easily understood by analyzing the properties of the various molecular orbitals. The orbitals of the square (4,4) are split into two blocks as was the case for the Pt_2–Pt_3 clusters. The block of lowest energy is mainly built from mixing the d atomic orbitals. The upper block is built from the interaction of sp atomic orbitals. A small mixing between the two blocks occurs via the sp–d interaction. As expected, this interaction is stabilizing for the lower d block and destabilizing for the upper sp block. This net block separation is abolished for the tetrahedron and the folded rhombus as it will be for larger systems: the energy gap between the d block

(20) Mehrotra, P. K.; Hoffmann, R. *Inorg. Chem.* **1978**, *17*, 2187. Dedieu, A.; Hoffmann, R. *J. Am. Chem. Soc.* **1978**, *100*, 2074. See also: Jordan, K. D.; Simons, J. *J. Chem. Phys.* **1976**, *65*, 1601.

(21) Cyrot-Lackmann, F. *J. Phys.* **1970**, *C1*, 67. Gaspard, J. P.; Cyrot-Lackmann, F.; Gordon, M. B. *J. Phys.* **1977**, *C2*, 57. Gordon, M. B.; Cyrot-Lackmann, F.; Desjonqueres, M. C. *Surf. Sci.* **1979**, *80*, 159.

and the sp block is progressively reduced as the size of the cluster increases. The Pt_4 series is the vanishing point. For the large clusters, the lowest sp level (mainly an in-phase combination of the s orbitals) is energetically lowered enough to pass below the highest antibonding d molecular orbital. This fact changes drastically the overlap population; the sp–d term is decreased sharply since an interblock out-of-phase mixing (the lowest orbital of the former sp block) replaces an interblock in-phase mixing (the highest orbital of the former d block). The two other terms (d–d) and (sp–sp) are relative to the intrablock phase relationship. Their values sharply change since the most bonding sp orbital is filled while the most antibonding d orbital is emptied. Since the s–s overlap at the MID is 3.8 times larger (0.176) than the best d–d overlap (0.046), a large s–s contribution to the overlap population is observed. The orbital interchange situation corresponds to the overlapping of the s and d bands in the language of solid-state physics. Henceforth, the position of the Fermi level is inside the d band for the compact clusters larger than Pt_4. The analysis of the total EHT + SO energy reveals the discontinuity in the overlap population. Indeed, the change in the relative SO contribution (30% vs. 18–25%) is associated with the change in the sp population which results from the orbital exchange phenomenon. It is interesting to note that the structures (4,1) and (4,5) have both the largest SO contributions of all the considered clusters and a large sp population which compares with that of much larger clusters (see Table IV). The above analysis of the Pt_4 cohesive energy does not change the conclusion on the relation between the optimal stability of the clusters and the maximum number of MIDs.

For the tetrahedron, as well as for many highly symmetric clusters, the highest d orbital belongs to a degenerate set. It is a Jahn–Teller situation, and a molecular distortion is expected to occur. This geometrical distortion should be small since any symmetry-breaking geometry change affects the sp–sp overlap more significantly than the d–d overlap. Consequently the energy of the highly stabilizing sp orbitals is affected more than that of the d orbitals. Thus, any deformation which removes the d orbital degeneracy will greatly reduce the stability of the whole system, forcing it to remain in a high spin state. The stability of the clusters with a zero gap between the frontier orbitals inducing a Jahn–Teller situation is a noteworthy exception to the Lauher rule.[3a] This exception may be a consequence of the unsaturated aspect of the pure platinum clusters.

Pt_5. Trapezium (5,1) with seven MIDs is the most compact Pt_5 planar structure. It is clear that it does not represent a stable species since it can lead to more compact structures, for example (5,2) or (5,4), by simple deformations which do not involve any bond breaking. Among the structures built from two CPTLs, the 3 + 2 possible arrangements gives two clusters with eight MIDs: the square pyramid P_4 (5,2) and an edged capped tetrahedron (5,3) which is also equivalent to a 4 + 1 arrangement as shown on Figure 1. This structure has not been calculated because it can be monotonously transformed into the trigonal bipyramid (5,4). Structure (5,4) is a 1 + 3 + 1 arrangement involving three CPTLs. It has nine MIDs, the largest number of the Pt_5 series. It has hcp packing and is the first polytetrahedron obtained by capping a triangular face of the tetrahedral structure (4,1). This capping leads to a gain of three MIDs for the new cluster. This gain is a general property in the generation of a Pt_n structure by aggregation of a single atom to a Pt_{n-1} cluster with external triangular faces.

Within class C, only the planar D_{5h} structure (5,5) has been calculated. With five MIDs, it has the smallest cohesive energy of all the structures considered in the Pt_5 series, as expected.

The energy of stabilization per MID in the Pt_5 series is, on the average, similar to what is observed in the Pt_4 series (approximately 0.58 eV per MID), except for the structure (5,2) which shows an extremum (0.62 eV). (5,2) is an example to what will be observed for other clusters presenting external square faces, i.e., high values of mean cohesive energy per MID.

Compared to the situation of the best Pt_4 clusters, the relative contribution of the SO coupling is reduced for the Pt_5 series. The origin of this reduction can be found in the decrease of the mean sp population (0.61 electron) relative to that of the best Pt_4 compounds (0.67 electron) and to the increase of local geometrical constraints which prevent optimal splitting of the orbital levels.

Pt_6. Let us first consider the Pt_6 isomers of class A. Three planar structures with nine MIDs can be generated. They are the equilateral triangle (6,1), the parallepiped (6,2), and the two-nested rhombi structure (6,3). From two CPTLs, a 3 + 3 arrangement generates the monoclinic trigonal prism or capped P_4 (6,4) with 11 MIDs and the octahedron (6,5) with 12 MIDs. These clusters are also 2 + 4 and 1 + 4 + 1 arrangements involving two and three CPTLs, respectively. Structure (6,5) can be considered as built from two P_4 with a common square face or as a triangular antiprism. In the latter sense, it initiates the series of antiprismatic structures of class C that we will consider for the larger clusters. For the first time, a compound of class B exists. It is the polytetrahedron (6,8) with 12 MIDs. It is built from three adjacent polytetrahedra sharing a common edge. Class C includes the trigonal prism (6,6) with nine MIDs and the pentagonal pyramid P_5 (6,7) with 10 MIDs.

The octahedron (6,5) is found to be the most stable system of the Pt_6 series, for which the order of stability is in agreement with the order of the mean coordination numbers (see Table III). To illustrate this point, let us consider (6,5) and (6,8). Structure (6,5) comes first and structure (6,8) in second position. Both structures have the maximum number of MIDs (i.e., 12), but they differ by the distances between their second-nearest neighbors. Indeed, for clusters of class A, the second-nearest neighbors are located at a distance 1.414 times larger than the MID, while for (6,8) the factors are 1.633 and 1.667. The lengthening of the 2.77-Å interatomic distance by factors 1.414 and 1.633 corresponds to a 64% and 98% decrease of the s–s overlap, respectively. Since the interaction energy is roughly proportional to the square of the overlap, it can be estimated that the extra stabilization energy brought by the second nearest neighbors is insignificant for (6,8) but is equivalent to 13% of the mean energy stabilization per MID for each of the three second-nearest-neighbor distances of (6,5). The calculated results (Table III) agree with these elementary considerations.

The sphericity of the octahedron (6,5) may also explain its high stability. Indeed, it fits within a small sphere of radius 1.96 Å. In a similar way, the exceptional stability of the tetrahedron (4,1) may be related to the small radius (1.70 Å) of its spherical envelope. It is worth noting that these two remarkably stable clusters are compact from both the point of view of the spherical density and the number of MIDs. No Pt_5 cluster matches both criteria simultaneously. Indeed, the Pt_5 cluster (5,4) with the maximum number (nine) of MIDs has a flattened shape which requires a large sphere of radius 2.26 Å while the Pt_5 cluster (5,2) with the largest spherical density (it fits within the sphere of (6,5)) has only eight MIDs. For this example, the highest number of MIDs has more influence on the cluster stability than the spherical density.

It is worth noting that the trigonal prism (6,6) has a stabilization energy significantly larger than would be expected by considering only its number of MIDs. Indeed, its cohesive energy per MID is 0.66 eV, while it is approximately 0.58 eV for the other structures as in the case of the clusters of the Pt_4 and Pt_5 series. This exceptional stabilization at the EHT level is a new example for the efficiency of sphericity (the sphere radius is small, 2.16 Å) and for the presence of external square faces.

For the Pt_6 series, the relative spin–orbit coupling contribution to the total cohesive energy is approximately 20%. The decrease compared with the preceding series comes from the increase in the local geometrical constraints for an identical or smaller d depopulation (see Table IV).

Pt_7. The centered hexagon (7,1) is derived from the planar structure (6,3) by addition of a Pt atom bonded by three MIDs. It is the first example of such an increase in the number of MIDs for the development of a planar structure. In fact, it is the usual step for the enlargement of a planar two-dimensional sheet of parallel atomic rows, except for the initiation of a new row, that

implies a gain of two MIDs. The fact that the gain of 3 MIDs per added atom has been shown to be a permanent possibility for the growth of any nonplanar cluster confirms the trivial conclusion that the compactness of a planar structure, and thus its stability, can never compete with that of the nonplanar isomers.

The consideration of all possible compact structures for clusters larger than Pt_6 would represent a tedious task. Thus, from now on, we will only consider the structures of class A with the maximum number of MIDs or with one MID less. Thus the Pt_7 structures examined in our study have 15 and 14 MIDs. The fit of two CPTLs with a 5 + 2 distribution gives the cluster (7,2), a bicapped P_4. The 4 + 3 distribution gives (7,3), the capped octahedron, and (7,4), another bicapped P_4. Only the (7,3) structure has 15 MIDs. The fit of three CPTLs with a 2 + 4 + 1 distribution gives an hcp derived structure (7,5). In class B, there are three polytetrahedra, (7,6), (7,7), and (7,8), which all have 15 MIDs. The n polytetrahedra can be generated from the $n - 1$ polytetrahedra by capping one of their triangular faces. This procedure cannot generate two extra tetrahedra in a single step since an atom cannot cap simultaneously two triangular faces belonging to two distinct tetrahedra. So, the capping of (6,8) to give (7,6) does not generate two regular tetrahedra but only one (the remaining cavity is a distorted tetrahedra with a distance equal to the 1.09 times the MID value). Therefore, the steps of the growth of the polytetrahedra are all similar. They add three MIDs to the $(n - 1)$ cluster. The formula $3(n - 2)$ gives the numbers of MIDs of the Pt_n polytetrahedra. That shows that the polytetrahedron series converges toward the same number of MIDs per atom as in the infinite planar sheet. However, the convergence is faster in the first case than in the second. In three dimensions, the maximum number of first nearest neighbors is 12.[22] This imposes a convergence to 6 for the number of MIDs per atom. This value is reached for the fcc or hcp bulk metals. Polytetrahedral growth is therefore not competitive.

Besides the polytetrahedra, another cluster, (7,9), belongs to class B. This cluster results from the sharing of a common face by a square pyramid (5,2) and a triangular bipyramid (5,4). Class C contains the D_{5h} bipyramid (7,10), which can be considered as resulting from a distortion of the polytetrahedron (7,6) by lengthening the edge common to its four tetrahedra. Class C also contains structure (7,11), derived from structure (6,8), by capping a square face of the trigonal prism. Structure (7,10) is a building block of the icosahedron Pt_{13} structure (13,33). Stricktly speaking, it has 15 MIDs, but the distance between the two apical atoms is 1.05 times the MID value. This distance may be counted approximately as an extra MID and makes (7,10) the most compact Pt_7 structure. The calculated energies show that (7,10) is the most stable structure and precedes (7,3) and the polytetrahedra, all with 15 MIDs (see Table III). The fact that the polytetrahedra are all less stable than the compounds of class A with the same number of MIDs can be related to the second nearest neighbor distances. They are larger for the polytetrahedra (except for one distance in (7,6)) than for the structures of class A. In the first case, the ratio with the MID is 1.633 while it is 1.414 in the second one. The consideration of repulsion for (7,10), as will be shown below, leads to an optimal geometry quasi-identical with the one described above with the usual minimal distance.

Within the Pt_7 series, the mean cohesive energy per MID is approximately 0.56 eV for all isomers, except for (7,11), which has a value of 0.66 eV. This isomer with only 13 MIDs has a cohesive energy larger than that of any isomer with 14 MIDs. Again, this exceptional cohesion can be related to the square open faces and to the sphericity (the sphere radius is 2.28 Å).

The mean value of the SO contribution decreases compared with the Pt_6 series, reaching 17%. The origin of this evolution is identical with that mentioned for the Pt_5–Pt_6 series.

Pt_8. The most compact Pt_8 structures have 18 MIDs. The fit of two CPTLs with a 4 + 4 distribution gives the three structures (8,1), (8,2), and (8,3). They can be considered as the matching of two rhombi Pt_4 structures (4,2). Structures (8,1) and (8,2) have the maximum number of MIDs and represent bicapped octahedra O_h. Structure (8,3) has a MID less and is made of $2P_4 + 2T_d$. The 5 + 3 distribution gives the structures (8,4), (8,5), and (8,6), which are made of $O_h + 2T_d$, and (8,7), which is made of $P_4 + 3T_d$. Only (8,4) has the maximum number of MIDs.

Let us now consider the various arrangements of three CPTLs. All the new structures are of the hcp type. The 3 + 4 + 1 distribution gives only the structure (8,4) already found. The 4 + 3 + 1 distribution gives, in addition to (8,2), (8,6), and (8,7), three new hcp structures: (8,8), (8,9), and (8,10). Only the first one has 18 MIDs and is a bicapped octahedron O_h. The distribution 2 + 5 + 1 gives (8,11) made of $P_4 + 3T_d$, in addition to (8,7) already described; the distribution 3 + 3 + 2 gives (8,12) made of $O_h + P_4$ and the 2 + 4 + 2 distribution gives, in addition to the structures (8,3) and (8,5) already found, (8,13) and (8,14) made of $2P_4 + 2T_d$.

In class B, we have the six possible polytetrahedra labeled (8,15)–(8,20). (8,15) has a T_d symmetry and is an all-capped tetrahedron. (8,17) and (8,18) can be considered as structures resulting from a distortion of the structure (8,21).

In class C, the structure (8,21) is derived from the D_{5h} bipyramid (7,10) by capping one of its triangular faces. It has 18 MIDs. Structure (8,22) is a square antiprism and has only 16 MIDs while the cube (8,23) has 12. Structure (8,24) with 17 MIDs is derived from the trigonal prism (6,6) by capping two of its three square faces.

Within the Pt_8 series, the order of stability does not strictly follow the order of compactness. Some structures with 17 and even 16 MIDs such as (8,24), (8,12), or (8,22) are more stable than structures with 18 MIDs. (8,21), the most compact structure, comes first at the EHT + SO level, but, surprisingly, the structure (8,24) with only 17 MIDs is the most stable cluster at the EHT level and remains quasi-degenerated with (8,21) after consideration of the SO coupling. (8,22) with only 16 MIDs and (8,24) with 17 MIDs have particularly high spherical density. Both structures have high cohesive energies per MID but small relative SO contributions. The presence of square open faces, existing in (8,24) as well as in (8,22), is well suited to generate a strong metal–metal bond at the EHT level as already mentioned. Both clusters (8,24) and (8,22) have larger overlap populations (0.1876) compared with the values of other clusters with the same number of MIDs or more (for example, (8,1) with 18 MIDs has a value of 0.165). This difference is mainly due to a larger sp–d in-phase mixing associated to the favorable local symmetry. The SO coupling acts as a local symmetry breaker and prevents this local symmetry from being fully effective at the EHT + SO level. Structures (8,10) and (8,12), which have external square faces, are other examples of clusters with relatively large cohesive energies at the EHT level but a small SO contribution at the EHT + SO level.

The polytetrahedra (class B) are less stable than the clusters of class A with the same number of MIDs. This can be explained by the second-neighbor interaction as in the case of Pt_7.

The cube (8,23) has a large mean cohesive energy per MID. This result can be attributed to the 12 second neighbor interactions at 1.414 times the distance of the MID as for (6,5).

For the first time, the cohesive energy of the six most stable isomers is within 0.10 eV. This result points out that, for the large clusters, it is not really possible to speak about the most stable cluster but about a quasi-degenerate ensemble.

Pt_9. Clusters of the Pt_8 series with 18 MIDs do not possess an external square face which can be capped to generate a compact Pt_9 cluster with 22 MIDs. They have only triangular faces. Their capping leads to Pt_9 clusters with a maximum number of 21 MIDs. Among the Pt_9 isomers of class A, only the structures with 21 MIDs will be considered. The fit of two CPTLs with a 5 + 4 distribution gives three clusters: (9,1), (9,2), and (9,3). The first two are tricapped octahedra, but the last one is $O_h + P_4 + T_d$ and has an external square face. The 5 + 3 distribution gives the structure (9,4), another tricapped O_h. The fit of three CPTLs with the 5 + 3 + 1 distribution gives (9,4), a structure already considered, while the 3 + 5 + 1 distribution gives (9,5) in addition

(22) Zemann, J. *Inorg. Chem.* **1963**, *324*, 241.

to (9,1). Structure (9,5) is made of $O_h + 3T_d$. Structure (9,6) is made of $2P_4 + 4T_d$ and results from a 2 + 5 + 2 distribution. The 1 + 4 + 4 distribution generates (9,7) and (9,8), in addition to structures (9,1) and (9,2) already found. The 3 + 4 + 2 distribution gives (9,9) in addition to (9,3) and the 3 + 3 + 3 distribution generates (9,10). Structures (9,7) and (9,8) are made of $O_h + 3T_d$, (9,9) is made of $O_h + P_4 + 2T_d$, and (9,10) is made of two O_h sharing a common face. The 1 + 4 + 3 + 1 distribution of four CPTLs gives a mixed-stacked structure (9,11) in addition to the hcp structure (9,2). Structure (9,10) has the lower energy among clusters of class A.

Class B contains 16 polytetrahedra which all have 21 MIDs. (9,21) and (9,22) have been computed as representative of this series.

Let us now consider structures of the class C. Five structures derived from (8,21) by capping two triangular faces of (7,10) can be generated. They are numbered (9,12)–(9,16); (9,13) is the most compact isomer. It is very close to a structure (9,13′), made of two irregular nested pentagonal bipyramids, which has a lower energy than (9,13). The structure (9,13′) has two short second-nearest-neighbor distances which, if included in the MID count, lead to 23 MIDs. Its cohesive energy is among the best for Pt_9 clusters. The structure (9,17) is derived from the square antiprism (8,22) by capping one of its square faces. It has 20 MIDs. The centered cube (9,18) has only eight MIDs, all involving the common central atom. This structure has a very small cohesive energy, associated with a large SO contribution (the local constraints are weak). Structure (9,19) can be considered as derived from the icosahedron (13,33) by removing four adjacent external atoms. This structure is very close to (9,13) and to the polytetrahedron (9,21); nevertheless, both structures are found to be less stable than (9,13′). Structure (9,20) is the most compact structure in the series initiated with the trigonal prism (6,6). It can also be considered as resulting from a distortion of the best structure of class A, (9,10). It is the most stable isomer of all the Pt_9 clusters.

It is striking that the monocapped square antiprism (9,17) with only 20 MIDs is more stable at the EHT level than all the structures with 21 MIDs except (9,20). After inclusion of the SO coupling interaction, its relative stability decreases and it is less stable than (9,10) and (9,13′). The structures (9,20) and (9,10) exhibit a good sphericity since they fit within spheres of small radius (2.56 and 2.77 Å, respectively). A cluster, (9,23), fits in a sphere of a even smaller radius (2.40 Å). This structure is an intermediate on the way from (9,10) to (9,20). It only has 18 MIDs and is found to be less stable than both structures (9,10) and (9,20). This result shows that compactness defined by the number of MID prevails over that defined by the spherical density for the stability of these clusters.

Except for (9,17) and (9,20), the mean cohesive energy per MID is quite constant within the Pt_9 series (0.53 eV). This value fits with the slow decrease observed in the other series when the cluster size increases.

Pt_{10}. Three Pt_9 clusters, (9,3), (9,6), and (9,9), have 21 MIDs and external square faces. Their capping leads to the Pt_{10} clusters with 25 MIDs. For example, the structure (10,1) is derived from (9,3) and the structure (10,3) from (9,9). Other aggregations of a single platinum to Pt_9 clusters can lead to an increase of four MIDs. For example, when the Pt_9 cluster has two external triangular faces that form an incomplete trigonal bipyramid (5,4) with a missing equatorial vertex, the filling of this position leads to an increase of four MIDs. The clusters (9,9) (one possibility) and (9,10) (three possibilities) illustrate this case and lead to the structures (10,2) and (10,3), respectively, in this way. The growth from (9,5) to (10,2) is another example of an increase of four MIDs. No other cluster of class A has 25 MIDs, but the clusters with 24 MIDs are numerous. The fit of two parallel CPTLs with a 5 + 5 distribution generates four clusters from (10,4) to (10,7), in addition to (10,1) already found. The 6 + 4 distribution generates (10,6) and three new structures: (10,8), (10,9), and (10,10). The 7 + 3 distribution leads to (10,11). The fit of three CPTLs with a 3 + 6 + 1 distribution generates the fcc cluster (10,12) and the hcp cluster (10,13). The 4 + 5 + 1 distribution gives, besides (10,6), (10,9), and (10,10), the fcc cluster (10,14) and four hcp clusters from (10,15) to (10,18). The 5 + 4 + 1 distribution generates two hcp clusters, (10,19) and (10,20), in addition to the clusters (10,4), (10,8), and (10,12) already found. The 3 + 5 + 2 distribution gives structures already generated in some other way: (10,2), (10,7), (10,9), (10,10), (10,11), and a new hcp structure (10,21). The 3 + 4 + 3 distribution gives the hcp structure (10,22) besides (10,3). The 5 + 3 + 2 distribution generates another hcp structure, (10,23), while finally the 4 + 4 + 2 trilayer generates three hcp structures, (10,24), (10,25), and (10,26), in addition to (10,6), (10,7), and (10,10).

The fit of four CPTLs gives some Pt_{10} clusters with 24 MIDs. The 1 + 4 + 4 + 1 distribution gives (10,4), (10,5), and four new clusters from (10,27) to (10,30). The 1 + 5 + 3 + 1 distribution gives (10,31) and (10,8), the distribution 1 + 3 + 4 + 1 gives (10,32), (10,33), and (10,6), and the distribution 1 + 3 + 3 + 3 gives (10,34). All the new clusters generated from four CPTLs are mixed-stacked structures except (10,27) and (10,30), which are hcp.

Numerous polytetrahedra can be generated and constitute elements of class B. They have 24 MIDs. It is the first time these clusters have less MIDs than the best structures of class A. Since they were significantly less stable with an equal number of MIDs, they will not be considered in detail for the Pt_{10} series.

Class C has a D_{4d} structure (10,35), which is derived from the square antiprism (8,22) by capping its two square faces. It has 24 MIDs. In class C, there are also (10,36) and (10,37), which can be considered as built either from the D_{5h} bipyramid and various polytetrahedra or from two or three nested irregular pentagonal bipyramids in a similar way as in (9,13′). Structure (10,37) is also derived from the icosahedron (13,33) by removing three adjacent external atoms. Those two last structures have 26 and 27 distances, respectively, which are of the order of the MIDs (between 2.77 and 2.92 Å). The D_{5d} antiprism (10,38) represents a new element in the series of the antiprismatic volumes. It can be considered as derived from the icosahedron with 12 platinum atoms (12,6) by removing two opposite atoms. The elimination of two opposite atoms from (12,6) is probably not the best choice to generate a Pt_{10} cluster since it removes 10 MIDs in a single step while the removal of two adjacent atoms would only remove 9 MIDs. However, such a process generates a large cavity in the cluster which prevents it from being a stable species. Structure (10,39) results from the capping of a triangular face of (9,20), the trigonal prism with all its square faces capped.

Among the 31 structures of class A with 24 MIDs, the computed values of 14 isomers are reported as representative of the main types of stacking (hcp, fcc, bilayers, trilayers, etc). These calculations show no clear-cut energetic distinction between the hcp and fcc clusters of the Pt_{10} series. When the structures of class A are compared at the EHT level, it is observed that all the structures with 24 MIDs are less stable than the structures with 25 MIDs. This order is no longer correct at the EHT + SO level since (10,34) precedes two clusters with 25 MIDs. At the EHT level, two structures of class C show a peculiar stability. They are the bicapped square antiprism (10,35) and the nearly fully capped trigonal prism (10,39), both with 24 MIDs. This last compound may be considered as resulting from a distorsion of (10,34) similar to the one discussed for (9,10) and (9,20). These structures fit in small spheres of radii (2.85 and 3.12 Å), and their stability is larger than expected by considering only their number of MIDs. Indeed, (10,35) is the most stable structure at the EHT level while (10,39) reaches an energy comparable to the energy of the best compounds of class A. The influence of the SO coupling changes the relative energies making these two compounds less stable than (10,1), the most stable structure at the EHT + SO level. After the (10,1) isomer, comes the bicapped antiprism (10,35) then the class A isomer (10,3) and the mixed stack (10,34), which, with 24 MIDs, is more stable than the structures (10,2), (10,36), and (10,39) with 25 MIDs.

Pt_{11}. Addition of a platinum atom to clusters (10,2) and (10,3) increases the number of MIDs by four to give an hcp-type

structure (11,1) with 29 MIDs. It is the only cluster of type A that contains 29 MIDs. Eleven clusters with 28 MIDs may be generated by the superposition of CPTLs: the 6 + 5 arrangement leads to (11,2) and (11,3), and the 7 + 4 arrangement leads to (11,4). From three CPTLs, the 2 + 6 + 3 sequence leads to an hcp structure (11,5); in addition to (11,1), (11,3), and (11,4), the 3 + 5 + 3 sequence generates the structure (11,8), while the 4 + 4 + 3 sequence generates, besides (11,2) and (11,3) already considered, two hcp structures (11,9) and (11,10); the 5 + 5 + 1 sequence gives (11,3) and an hcp structure (11,11). The four CPTLs superposition gives (11,2) from the 1 + 3 + 4 + 3 sequence and a mixed-stacked structure (11,12) by using a 1 + 3 + 5 + 2 sequence.

The polytetrahedra for Pt_{11} have only 27 MIDs. They are less compact than clusters considered in class A. The structure (11,13) has been computed as representative of this group of clusters. Structure (11,14) is derived from (7,10) by capping four triangular faces.

Class C includes a structure (11,15) derived from icosahedron (12,6) by removing one platinum and a structure (11,16) derived from the icoshedron (13,33) by removing two platinums. The first one has 25 MIDs and the second only 10. They have small cohesive energies compared to the other structures considered. The most stable cluster at the EHT level is (11,1), i.e., the cluster with the largest number of MIDs. At the EHT + SO level, this cluster is relegated to the third place, after (11,2) and (11,3). The origin of this inversion can be found from the fact that (11,1) is a trilayer cluster while (11,2) and (11,3) are bilayers having reduced local geometrical constraints, favoring the SO coupling. Furthermore, (11,2) and (11,3) have larger "sp" densities than (11,1), which favors the SO coupling stabilization (17% and 16%, respectively vs. 15% for (11,1)).

Pt_{12}. The cluster (11,1) possesses a square face. Its capping gives four supplementary MIDs leading to (12,1), which is the only structure with 33 MIDs. Four clusters of class A have 32 MIDs: the bilayer structure (12,2) comes from a 7 + 5 arrangement, (12,3) and (12,4) are hcp structures generated by a 3 + 5 + 4 arrangement of three CPTLs, and the four layer 1 + 5 + 3 + 1 sequence gives the mixed-stacked structure (12,5). The other three CPTL arrangements gives structures already obtained: (12,2) comes from the 2 + 5 + 5 or 3 + 5 + 4 sequence and (12,1) from the 3 + 6 + 3 sequence. A structure of class A with 31 MIDs has been computed. It is (12,9), which results from the removal of an atom from the cuboctahedron (13,4).

Class C includes a remarkably highly symmetric D_{5d} structure, the icosahedron (12,6) with 30 MIDs. This compound has a cavity that could almost fit an extra atom to generate the Pt_{13} icosahedron (13,33). Among all the possible polytetrahedra, the structure (12,7) has been selected since it appears as one of the most compact. It is derived from (11,13) by capping a tetrahedron and has 30 MIDs. Small distortions of this structure gives the highly symmetric C_{5v} all-cis-capped pentagonal bipyramid (12,8) as well as the structure (12,12) obtained by removal of an outside atom from the icosahedron (13,33). Structure (12,8) has 30 MIDs while (12,12) has 11 MIDs and 25 interatomic distances with a value 1.05 times larger than the MID. In spite of the large number of interatomic distances in the range of the MIDs, this structure has a cohesive energy that does not compare with the other isomers considered. The D_{4h} structure (12,10) is made of three parallel square planes and is an extension of the square antiprism (8,22). It has 28 MIDs. The last structure considered in the Pt_{12} series is (12,11), which is the all-capped square face rhombus prism. It has 30 MIDs.

At the EHT level, the most stable structure (12,6) is the icosahedron although it does not have the largest number of MIDs. Structure (12,6) fits in a small sphere (radius 2.63 Å). At the EHT + SO level, the relative cohesion of this structure is greatly reduced since it only comes at the seventh place. The bilayer structure (12,2) is found to be most stable. The strong variation in the influence of the SO coupling can again be attributed to the difference in the "sp" density [0.61 for (12,5), 0.60 for (12,2), and only 0.50 for (12,6)] and to the difference of flexibility in the local geometry [(12,6) has only atoms with five bonds while (12,2) has four atoms with four bonds].

Pt_{13}. Structure (12,1), the Pt_{12} cluster with the largest number of MIDs, has only external triangular faces. If one of these faces is capped, it gives two Pt_{13} cluster with 36 MIDs. They are the structures (13,1) and (13,2). Structure (13,1) is a 3 + 6 + 4 hcp arrangement of three CPTLs, and (13,2) a 3 + 6 + 3 + 1 mixed-stacked arrangement of four CPTLs. The same number of MIDs is obtained by capping the square faces of (12,2) and (12,9) to give (13,3), a 7 + 6 bilayer, and (13,4), the fcc cuboctahedron that is also derived from a 3 + 7 + 3 sequence. An identical sequence gives (13,5), the anticuboctahedron that belongs to the hcp growth. Cuboctahedron and anticuboctahedron are derived from cluster (10,11) by the addition of a three-atom cluster (3,1), introducing 12 MIDs at once. The successive addition of single atoms to (10,11) with +3 MIDs first, +4 MIDs next, and +5 MIDs last, leads to the Pt_{11} and Pt_{12} structures of nonmaximum compactness. So, the step growth appears less favorable than the coalescence of the clusters (3,1) and (10,11) to generate (13,4) and (13,5).

Twenty-seven clusters with 35 MIDs, a MID less than the clusters so far mentioned, belong to class A. Let us now describe them. From two CPTLs, the 6 + 7 arrangement leads to two new clusters, (13,6) and (13,7), while the 8 + 5 arrangement leads to (13,8). There are many ways to match three CPTLs. The 3 + 7 + 3 sequence gives two clusters, (13,9) and (13,10); (13,9) is an fcc stack, and (13,10) is an hcp one. The 2 + 7 + 4 sequence gives three clusters (13,11)–(13,13). The first one is fcc, but the others are hcp. The 1 + 7 + 5 sequence gives four clusters numbered from (13,14) to (13,17); the first two are fcc and the two last are hcp. The 7 + 5 + 1 sequence of three CPTLs gives a fcc structure (13,18) and an hcp structure (13,19). The 3 + 6 + 4 arrangement leads us to rediscover many fcc structures, (13,6), (13,9), (13,11), (13,14), (13,15), and (13,18) as well as an hcp structure (13,1); it also generates three new hcp structures, (13,20), (13,21), and (13,22). The 2 + 6 + 5 sequence gives the new hcp structures (13,23) and (13,24), in addition to the already described structures (13,1) and (13,14). The 6 + 5 + 2 sequence gives (13,8) and (13,18), which are not new structures. The 5 + 5 + 3 sequence gives, in addition to the structures (13,3), (13,8), (13,15), and (13,18), three new hcp clusters (13,25), (13,26), and (13,27). Finally, the 4 + 5 + 4 sequence generates five new hcp structures from (13,28) to (13,32) plus the three known clusters (13,6), (13,13), and (13,14).

Icosahedron (13,33) is the last term of the extension of nested pentagonal bipyramids. Its nearest-neighbor distances can be divided into two distinct sets. One has the value of the MID; there exist the 12 such bonds. The other has a slightly increased value (1.05 times the MID as already pointed out); there are 30 such bonds. By counting all these bonds as MIDs, we get 42, a significant increase compared with the most compact structures of class A. However, strictly speaking, (13,33) has only 12 MIDs. The fact that the cohesion of the icosahedron is far behind that of structures with 36 or even 35 MIDs shows how fast the interaction falls off with an increase of the interatomic distance around the MID.

Three structures of D_{5h} symmetry can be built. Structure (13,34) is the union of two polytetrahedra (7,6) which shares a common apical vertex. It has 35 MIDs and two other nearest-neighbor distances at 1.09 times the value of the MID. Structure (13,35) is the union of two pentagonal bipyramids which shares a common apical vertex. It has 30 MIDs plus seven nearest-neighbor distances at 1.05 times the value of the MID. The shortening of the distance between the equatorial planes leads to structure (13,36) with 20 MIDs and 17 nearest-neighbor distances at 1.01 times the value of the MID.

The last structure considered, (13,37), is a 3 + 3 + 3 + 3 cluster with MIDs. It is an hcp stack which could be considered as the union of two octahedra sharing a common face.

In class A, all the structures with 36 MIDs, but only nine structures with 35 MIDs, have been computed. The isomers with 35 MIDs have been selected as exemplifying the various possi-

bilities as it was done for the Pt_{10} series.

The structure with the largest cohesive energy at the EHT level is (13,5). The structure (13,4) is quasi-degenerate with (13,5). Next, come (13,3) and structures with 35 MIDs ((13,37), (13,23), (13,34), (13,21)) which are more stable than the two last structures with 36 MIDs, (13,1) and (13,2). So, the order of stability does not fully follow the order of compactness. Structures (13,4) and (13,5) are remarkably spherical. They fit within a sphere of radius 2.77 Å. At the EHT + SO level, structures (13,5) and (13,4) are less stable than clusters (13,3), the most stable one, and (13,23). The reasons for these inversions are similar to what was mentioned above (i.e., a large difference in the sp population and different local geometry constraints).

Beyond Pt_{13}. Beyond Pt_{13}, the maximum number of MIDs increases regularly. There is always a possibility of adding an atom introducing four MIDs at once. Cuboctahedron and anticuboctahedron have six square faces. That ensures a gain of four MIDs for their successive cappings. Cuboctahedron (13,4) leads to (19,1) in that way, by giving successively (14,1), (15,1), (16,1), (17,1), and (18,1). Structure (19,1) has 60 MIDs and is built from three CPTLs in a 6 + 7 + 6 arrangement. It is an octahedron which has eight triangular faces made of six atoms such as in (6,1). The addition of eight clusters (3,1) on each of these faces, in a manner similar to the way (6,1) gives (9,4), leads to a cluster of 43 metal atoms with 156 MIDs, (43,1), representing 3.63 MID per atom. Structure (43,1) is noticeable since it has 12 empty sites corresponding to 5 MIDs. Their occupation leads to a cuboctahedron (55,1) with 55 atoms and 216 MIDs (an average of 3.93 MID per atom). The existence of external (100) surfaces leads us to think that isomers with external (111) surfaces and a larger number of MIDs are available (see infra). Clusters (43,1) and (55,1) belong to class B. In a similar way as (13,4) leads to (19,1), the anticuboctahedron (13,5) leads to a Pt_{19} structure (19,2) with 60 MIDs. This growth generates an anticubocathedron of 55 atoms. An icosahedron of 55 atoms may also be constructed as an isomer of (55,1). The structure (13,3) can also be expanded with an increase of 4 MIDs per atom by the addition of a (3,1) cluster on the seven-atom face. This leads to (16,2) with three CPTLs (arrangement 3 + 6 + 7) and a T_d symmetry, each face being either a regular centered hexagon or a triangle. On each hexagonal face, it is possible to add a triangular six-atoms cluster (6,1). This addition induced an average progression of four MIDs per atoms. The first addition of three atoms gives (19,3), and the complete coverage yields the cluster (40,1). This cluster is of class B and has 144 MIDs (3.6 MID per atom). This structure has four empty sites associated with 6 MIDs. The addition of four atoms in these sites generates a cluster (44,1) of 44 atoms and 168 MIDs, i.e., 3.82 MIDs per atom. All the structures (19,1), (19,2), (19,3), (40,1), (43,1), (44,1), and (55,1) have high spherical density.

Another interesting growth starts from the structure (20,1), which has 63 MIDs and is made of two fused cuboctahedra. It corresponds to a fcc arrangement (5 + 10 + 5) of three CPTLs and has the same number of MIDs as the Pt_{20} cluster derived by capping (19,1). The capping of all its square faces leads to a Pt_{28} cluster (28,1), which is a 9 + 10 + 9 arrangement of three CPTLs and has 97 MIDs (3.46 MID per atom). The cluster (28,1) has four trapezoidal faces with nine atoms and four triangular faces with six atoms. The coverage of the trapezoidal faces by clusters (6,1) leads to a Pt_{52} cluster with 203 MIDs which has four empty pentacoordinated sites. Filling three of them gives a Pt_{55} cluster with 218 MIDs, two MIDs more than (55,1). No cluster larger than Pt_{19} has been computed.

From these simple examples of nucleation, it is obvious that the convergence of number of MIDs per atom toward 6, the value of the bulk, is slow with the growth of the clusters. Indeed, the average number of MIDs per atom remains below 4 up to 55 atoms. The values for infinite systems is 3 for a CPTL, 4.5 for a bilayer, and more generally $(6n - 3)/n$ for a fcc, hcp, or mixed stack of n layers.

Infinite Systems. Calculations of different periodic systems are presented in Table V. First, two one-dimension chains are considered: one is the infinite Pt_6 ribbon generated by the translation of an octahedron (6,5) along its C_3 symmetry axis. This axis becomes a screw axis for the Pt_6 ribbon. This volume extension of (13,37) has an antiprismatic pattern. The other is the infinite Pt_4 ribbon. It is an extension of (8,1) since it is generated by the translation of the planar rhombus (4,2) in such a way that the different rhombi exist in parallel (111) planes of an fcc packing. Next, there are the two-dimension systems or multilayers: they are the one, two, and three parallel (100) layers of an fcc packing. In each layer, the platinum atoms form a square lattice. There are also the various fcc, hcp, or mixed parallel (111) layers obtained from the matching of one–nine CPTLs. The three-dimensional systems studied are the fcc and the hcp packing of the metal. All these periodic systems have numbers of MIDs per atoms which go from 2 to 6 as shown in Table V. For the packing of CPTLs the number of MIDs varies from three for the (111) monolayer to the bulk. The cohesive energy per atom increases rapidly from 1.35 to 2.02. In all the cases, the fcc and hcp (111) stackings have very similar energies. For the monolayer the cohesive energy represents only 68% of the cohesive energy of the bulk; the bilayer reaches 84% and the trilayer 90%. The cohesive energy per MID decreases smoothly. It is noteworthy that the values for the infinite systems remain close to the values of the clusters for an equivalent number of MIDs per atom. The (100) monolayer can be compared with clusters (6,5) and (6,8), while the monolayer (111) and the ribbon Pt_6 are slightly better than the compounds (16,1) and (16,2).

Table V. Calculated Energy Data on Infinite Systems

	no. MIDs per atom nm	EHT	EHT/ nm	EHT + SO	(EHT + SO)/nm	%SO
chain Pt_6	3.00	1.3266	0.44	1.5343	0.51	13.5
chain Pt_4	3.25	1.2373	0.31	1.4942	0.46	17.2
(100) plane						
1 layer	2.00	0.8964	0.45	1.2107	0.62	26.1
2 layers	4.00	1.613	0.40	1.8475	0.46	12.7
3 layers	4.17	1.7261	0.38	2.0239	0.43	14.7
(111) plane						
1 layer	3.00	1.3480	0.45	1.5586	0.52	13.5
2 layers	4.50	1.7143	0.38	1.9319	0.43	11.3
3 layers fcc	5.00	1.8072	0.36	2.0618	0.41	12.4
3 layers hcp	5.00	1.8009	0.36	2.0693	0.41	13.0
4 layers fcc	5.25	1.8671	0.36	2.1251	0.40	12.1
4 layers hcp	5.25	1.8546	0.35	2.1219	0.40	12.6
4 layers mix	5.25	1.8597	0.35	2.1203	0.40	12.3
5 layers fcc	5.4	1.8952	0.35	2.1557	0.40	12.1
5 layers hcp	5.4	1.8806	0.35	2.1522	0.40	12.6
6 layers fcc	5.5	1.9162	0.35	2.1799	0.40	12.1
7 layers fcc	5.57	1.9320	0.35	2.1963	0.39	12.0
9 layers fcc	5.67	1.9525	0.34	2.2172	0.39	11.9
fcc bulk	6.00	2.0232	0.34	2.2918	0.38	11.7
hcp bulk	6.00	1.9895	0.33	2.2596	0.37	12.0

The sp density per atom increases from 0.83 to 0.95 for the (111) multilayers; conversely, the SO coupling increases from 0.21 to 0.27 eV. It, however, corresponds to a relative decrease of the SO contribution. Per MID, the sp density decreases from 0.28 to 0.16 and the SO contribution falls from 13.5% (in the (111) monolayer) to 11.7% (in the fcc bulk). The (111) monolayer is found to be more stable than the (100) monolayer. This result is consistent with the order of densities. Structure (111) has 3 MIDs per atom while (100) has only 2. It is interesting to note that the (100) layers have higher SO coupling contributions than the (111) layers. It is peculiarly striking for the monolayer. The high SO contribution (26%) is not explained by the sp population (0.62). For a comparable sp population and a same number of MIDs per atom, the SO contribution accounts for 18% in the compound (6,5). This high SO contribution for the (100) layer comes from the weak geometrical constraints of the lone plane. This conflicts, however, with the general observation that the presence of square faces on clusters did not lead in general to a large SO term.

For the bulk metal, the fcc stacking is found to be more stable than the hcp stacking. The cohesive energy per platinum is 2.023 and 2.292 eV at the EHT and EHT + SO levels, respectively, for the fcc stacking. These values are the upper limits for the computed clusters. The stabilization due to the SO coupling represents 11.7% of the cohesive energy. This value is in agreement with the results published by Cyrot-Lackmann et al.[21] The hcp stacking has a cohesive energy of 1.990 and 2.260 eV at the EHT and EHT + SO levels, respectively. For all the infinite systems, the SO coupling is found to favor the hcp systems, even if those do not become more stable than the fcc ones. This was not always the case for the clusters, one example being the cuboctahedron (13,4), which is more stable than the anticuboctahedron (13,5) after the SO coupling contribution is included.

Experimentally, it is found that the most stable packing of the metallic platinum in the solid state is fcc. The heat of atomization[2a] is found to be 5.85 eV per atom at 25 °C. This value corresponds to a final system with the single atoms in their ground state. It is not directly comparable to the EHT partition of the cohesive energy.

Consideration of the Short-Range Repulsive Interactions. So far, all structures presented have a common value for the distances separating the first-nearest-neighbor atoms, the MID. For most of them, the direct interaction with atoms other than their first nearest neighbors is negligible, because the second-nearest-neighbor distance (SND) is large compared with the MID (usually 1.414 MID). Some clusters, however, have SND that are only slightly larger than the MID. The structures (7,12), (8,25), (9,19), (10,37), (11,16), and (12,12), derived from the icosahedron (13,33) by removing the appropriate number of adjacent atoms, have this property. The number of their SNDs is significant when it is compared with the number of their MIDs: 12 and 30 respectively, for (13,33). In the series (7,10), (8,21), (9,12)–(9,16), and (10,36), however, the number of small SNDs is always relatively low: one SND and 15 MIDs for (7,10), two SNDs and 21 MIDs for (9,13). The correction is expected to be weak in the case of a low relative number of SNDs since the destabilization due to the compression of many MIDs opposes the shortening of one or two SNDs.[22] To get quantitative information on the possible distance relaxations, we tested various distortions on (7,10) and studied the series (7,12)–(13,33) in detail by performing geometry optimizations with the introduction of short-range repulsive contributions in the classical EHT program.

Let us first consider the correcting method which involves a modification of the H_{ij} interacting term by a factor $1 - \exp(a - bR)$. Three sets of parameters a and b have been selected by imposing a first-nearest-neighbor distance of 2.77 Å in the cuboctahedron (13,3). The cuboctahedron is a member of class A. It has been found that whatever the selected parameters are (Table VI), they do not induce significant distance changes for the other compounds of the same class. For example, the interatomic distances of the Pt_2 dimer and the Pt_4 tetrahedron are equal to the fixed value of the MID (2.77 Å) within 0.01 Å. This result clearly shows that, in class A, the second-nearest-neighbor distance (1.414 times the first-nearest-neighbor distance) creates no significant repulsive contribution.

For (7,10), the optimization is supposed to shorten the apical distance. However, because it induces the concomitant shortening of 15 nearest-neighbor distances, the apical shortening is expected to be small. Two optimizations have been considered. One scales down the whole structure by a common factor, the other increases the peripherical equatorial bonds and decreases the apical distance while it holds constant the length of the other bonds. The latter situation is the most favorable, but it does not significantly affect the initial structure since it requires that we increase five bond lengths while reducing only one. The calculations are in agreement with this deduction since the optimal apical distances are found to be equal to 2.76, 2.77, and 2.77 Å for the three sets of parameters, respectively. For compounds such as (7,10), the consideration of the fixed value of the MID seems justified.

The other clusters of the series (7,12)–(13,33) have more flexibility. Table VI gives the optimized distances and energies for the three sets of parameters. It shows that the smallest interatomic distances can be significantly affected (0.08 Å for the largest change) and that the optimized structures remain less stable than their reference isomer, even if the difference is reduced significantly. The icosahedron has 12 internal interatomic distances which have to be shortened to a value smaller than the fixed MID in order to reduce the 30 external interatomic distances (2.92 Å). Table VI shows that the internal distances are reduced to 2.75, 2.72, and 2.69 Å for the different parameter sets. Cyrot-Lackmann et al. reported a computed value of 2.71 Å.

Table VI. Interatomic Distances and Energies with the Corrected Hamiltonian $H_{ij}^* = H_{ij}(1 - \exp(a - br))$[a]

compd	set 3	set 2	set 1	direct EHT
(13,33)	2.89/2.75	2.86/2.72	2.83/2.69	
(13,14)	0.953	0.561	0.160	1.30
(12,12)	2.88/2.74	2.87/2.73	2.85/2.71	
(12,1)	0.850	0.533	0.144	3.84
(11,16)	2.88/2.74	2.87/2.73	2.85/2.71	
(11,1)	1.041	0.758	0.414	3.64
(10,37)	2.88/2.74	2.86/2.72	2.85/2.71	
(10,35)	1.129	0.880	0.555	3.22
(9,19)	2.88/2.74	2.88/2.74	2.86/2.72	
(9,20)	1.065	0.851	0.578	2.65
(8,25)	2.88/2.74	2.88/2.74	2.86/2.72	
(8,24)	0.929	0.754	0.507	1.24
(7,12)	2.86/2.72	2.89/2.75	2.86/2.72	
(7,10)	0.761	0.605	0.354	1.01

[a] The values for three sets of parameters (39.375/15.75, 70.2/27, 119.25/45) are reported; r is in angstrom. For each optimized structure, the table contains the values of the two first-nearest-neighbor distances in angstroms and the energy difference in eV with a reference isomer of class A. For each set of isomers, the first line gives the numbering of the optimized structure and its optimized distances; the second line gives the numbering of the reference compound and the energy difference.

Table VII. Interatomic Distances and Energies with the Two-Step Correction $E = E(\text{EHT}) + \sum \exp(c - dr)$[a]

compd	set 1	set 2	set 3	set 4
(13,33)	2.92/2.78	2.86/2.72	2.86/2.72	2.86/2.72
(13,3)	1.6155	0.5668	0.1832	0.1244

[a] The values for four sets of parameters (634.12/231.05, 60.42/23.10, 29.11/11.55, 18.85/7.07) are reported; r is angstrom. For the optimized structure, the table contains the values of the two first-nearest-neighbor distances in angstroms and the energy difference in eV with the reference isomer of class A (13,3). The first line gives the optimized distances and the second line the energy difference.

The second correction technique of the classical EHT method has been applied to the comparison between the icosahedron and the cuboctahedron (13,3). This two-step correction requires that we substract a repulsive contribution of $36 \exp(c - 2.77d)$ eV from the classical EHT cohesive energy of (13,3) and a contribution of $12 \exp(c - dr) + 30 \exp(c - 1.05dr)$ from the classical EHT cohesive energy of (13,33) where r is the internal distance of the icosahedron. The results are reported in Table VII for the four selected sets of parameters c and d. In all cases, the cuboctahedron remains the most stable isomer.

These results show that the constraint of a fixed value for the first-nearest-neighbor distance does not prevent us from finding the correct order of stability for the platinum clusters.

5. Discussion

The first point to discuss is concerned with the influence of the SO coupling for the various clusters and infinite systems. Although the introduction of the SO coupling affects the energy of all the EHT orbitals, the total energy changes only if the $\hat{L}\hat{S}$ mean value is not zero. When the electronic population of a given atom differs from d^{10}, this atom has a nonzero contribution to the $\hat{L}\hat{S}$ value according to the importance of its d depopulation (or equivalently of its sp atomic population). As the atomic d population is related to the cluster geometry, the importance of the SO effect is geometry dependent. Usually, the large differences in the SO

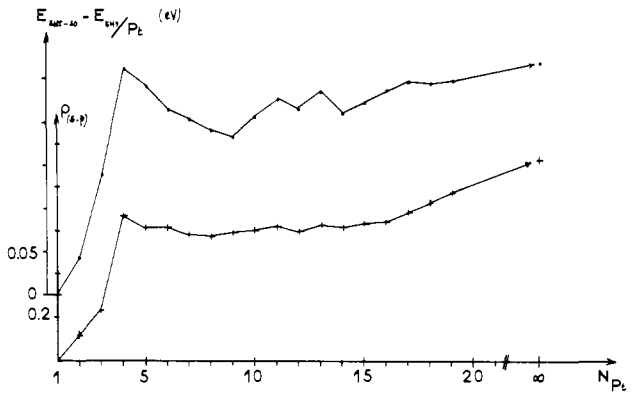

Figure 2. Lower curve: plot of stabilization energy per atom brought by the spin–orbit coupling vs. the number of platinum atoms in the clusters. Upper curve: plot of the "s-3p" electronic density per atom vs. the number of atoms in the clusters.

contribution could be related to those in the sp population. For example, (11,2) and (11,1) have a SO contribution of 0.408 and 0.125 eV, respectively; the sp population of (11,2) is 0.38 electron larger than the corresponding population of (11,1).

The stabilization energy per atom induced by the SO coupling (the difference between the EHT + SO and the EHT energies) and the sp population per atom as a function of the number of atoms are reported in Figure 2 for the most stable clusters. Both curves show a sharp increase from Pt_1 to Pt_4. From Pt_4 to Pt_9, a smoother decrease is observed. This decrease is more pronounced for the SO energy than for the sp electron density. From Pt_9 to the bulk, both curves show small oscillations with extremum for the same dimension of the clusters. It is interesting to note that the density curve is quite flat between Pt_5 and Pt_{15} (the density is between 0.61 and 0.63 electron), but it has a steep increase starting at Pt_{16}. Indeed, the sp density goes from 0.64 to 0.78 electron when the cluster grows from Pt_{16} to Pt_{19} By estimating that this increase in rate will continue up to the value of the bulk, we see that clusters around Pt_{25} have already an sp density comparable to the bulk metal. If we consider that a given sp population is a specific property of the bulk metal, clusters as small as Pt_{25}–Pt_{30} will have quite similar electronic properties with the bulk metal.

A more detailed analysis of the sp population has been done for various clusters and infinite systems (see Table VIII) in order to see how this population varies with the surrounding atoms. Table VIII shows that the internal atoms of infinite sheets have sp populations that are similar to those of the bulk metal. This property is true even for a trilayer system. Thus according to this result, the atoms located in the layer just below the surface already have the electronic properties of the atoms in the deep bulk. The atoms of the surface behave quite differently since their sp population is reduced by 0.1–0.2 electron compared with the bulk atoms and since they are negatively charged (–0.1, –0.2 electron) while the atoms in the internal layers are all positively charged (up to 0.2 electron). Interestingly, these properties are observed for clusters such as (19,1). The outer atoms have an sp population of 0.64 electron, and the internal one has a population of 0.94 electron.

The d orbital population is not, however, the only factor that determines the importance of the SO coupling on the total energy. Indeed, for two metallic systems with identical sp orbital populations but different geometries, the influence of the SO term is different. This is due to the fact that some geometry patterns fit better than others the simultaneous symmetry requirements of the electrostatic and SO coupling interactions. Precisely, some local geometries, while exceptionally stable at the EHT level, appear to be relatively unfavorable for the SO coupling. The Pt_4 square skeleton appears to be such an example. The octahedron (6,5), the capped trigonal prisms (7,11) and (8,24), the octahedron-derived structures (8,10), (8,12), (9,9), and (9,10), and the square-derived structures (8,22), (9,17), and (10,35) illustrate this finding.

Table VIII. Net Charges and "s-3p" Densities for Each Layer of the Two-Dimension Infinite Systems[a]

multilayer		external layer	second layer	third layer	fourth layer
3 layers	(100)	−0.0961	+0.1921		
		0.841	0.957		
3 layers	(111)	−0.108	+0.216		
	fcc	0.921	0.969		
	(111)	−0.088	+0.196		
	hcp	0.879	0.967		
4 layers	(111)	−0.165	+0.165		
	fcc	0.865	0.955		
	(111)	−0.166	+0.166		
	hcp	0.885	0.960		
	(111)	−0.185/−0.195	+0.190		
	mix	0.871/0.875	0.956/0.954		
5 layers	(111)	−0.137	+0.067	+0.141	
	fcc	0.862	0.942	0.958	
5 layers	(111)	−0.169	+0.134	+0.066	
	hcp	0.851	0.923	0.924	
6 layers	(111)	−0.199	+0.047	+0.153	
	fcc	0.910	0.893	0.972	
7 layers	(111)	−0.194	+0.020	+0.120	+0.110
	fcc	0.873	0.958	0.962	0.951

[a] The charges are in electron per atom. The first line gives the total net charge and the second the "s–3p" population density.

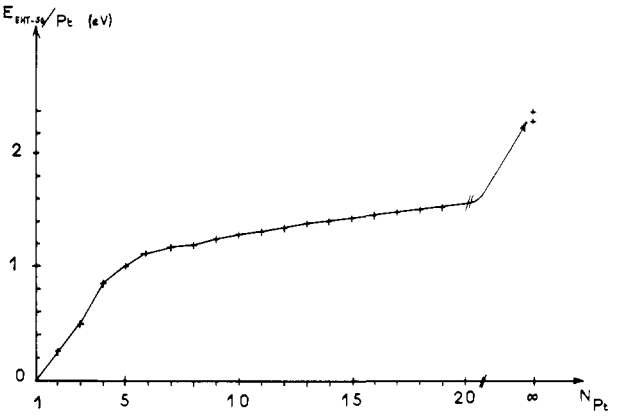

Figure 3. Plot of the cohesion energy per atom at the EHT–SO level vs. the number of platinum atom for the most stable clusters.

SO coupling acts as a local symmetry breaker and mixes together occupied and vacant orbitals. It is expected that the SO coupling will noticeably reduce the energy gap between the occupied and vacant orbitals whenever a large gap at the EHT level is due to symmetry factors. Since a large gap is generally associated with a large cluster stability,[3a] it is understandable that the SO coupling, by decreasing all the energy gaps, reduces the differences between the stability of the symmetric (large) gaps and those with lower symmetry.

It appears that the increases of geometrical constraints and of sp population with the coordination number play balanced roles. The value of the SO contribution per platinum indeed shows no clear trend on going from Pt_4 (0.26 eV) to the crystal bulk (0.27 eV), passing by lower values as 0.18 eV for Pt_7 or Pt_9. Since the cohesive energy per platinum increases with cluster size, the relative contribution of the SO coupling to the total energy decreases from 30% to 12% in going from Pt_5 to the metal bulk while the sp population increases from 0.64 to 0.95 electron (Tables III and V).

Let us now consider the general features of the cluster growth as depicted in the previous section. In Figure 3, the cohesive energy per platinum is represented as a function of the number of atoms. It shows a sharp increase of this energy up to Pt_6 and a smooth regular increase for the larger clusters. Figure 3 shows that, as expected, the mean value for the Pt_{19} clusters are still far smaller than that for the bulk since there are only a few atoms having their 12 neighbors. In Figure 4, the same cohesive energy per atom is drawn as a function of the mean number of MIDs per

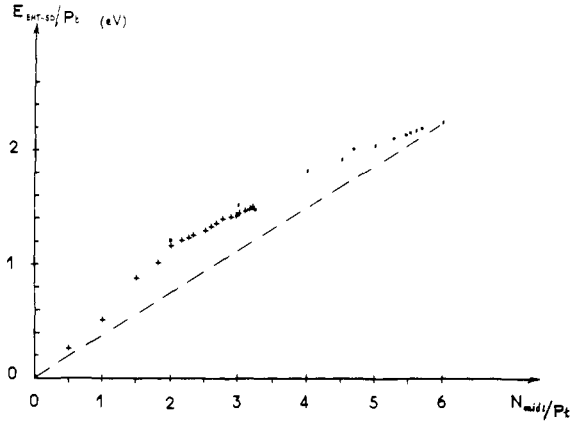

Figure 4. Plot of the cohesion energy per atom at the EHT–SO level vs. the mean number of MIDs per platinum atom for various clusters (×) and infinite systems (○).

atom. It shows that the cohesive energy is roughly proportional to the mean number of metal–metal bonds engaged by each atom. More precisely, Figure 4 shows that the clusters have some extra stability compared with the mean value for the bulk. The metal–metal bond, on the average, is stronger in the cluster than in the bulk metal. The systems with the stronger bonds are clusters with a number of MIDs between two and four. This result could explain why it is found that small coordinatively saturated clusters can form quite stable molecular entities since the metallic framework is quite strongly bonded. An interesting feature of Figure 4 is that the finite clusters and the infinite systems with the same mean number of MIDs per atom have the same mean cohesive energy. This reinforces our conclusion that a key factor in stability of metallic systems is the number of bonds per atom they have, regardless of detailed geometrical patterns.

Figure 5 shows the enthalpies of the reactions $Pt_{n-1} + Pt \rightarrow Pt_n$ as a function of n, where the dimension of the clusters refers to the most stable isomers. These reactions could imply a large reorganization of the metallic structure. The figure shows that in general the addition of an atom to any Pt_n cluster is always exothermic. This result does not offer any indication on the energy profile of the possible reaction paths for such a process. However, in agreement with the Hammond postulate, it is reasonable that the most exothermic reaction would correspond to the kinetically more feasible process.

At the EHT level, the successive enthalpies of the cluster growth present three maxima for $n = 6$, 9, and 13. These clusters have high symmetries and large spherical densities.

To analyze in more detail the influence of the spherical density on stability, let us consider the growth of the enveloping sphere with the cluster size. The maximum sphericity sequence and the associated radii are (4,1)/1.70, (5,2)/1.96, (6,5)/1.96, (7,10)/2.36, (8,22)/2,28, (9,23)/2.40, (10,38)/2.63, (11,15)/2.63, (12,6)/2.63, and (13,4-5)/2.77 Å. All these clusters have large cohesive energies per MID. They are not, however, in all cases the most stable isomers since some of them have relatively low numbers of MIDs ((5,2), (8,24) (9,23), (10,38), (11,15)). The most stable clusters tend to have a large spherical density and a high number of MIDs simultaneously. These are (4,1), (6,5), (9,20), and (13,4-5). Thus, the consideration of the spherical density allows us to understand the observed extrema of Figure 5. It also explains the extrema for the mean energy per MID. For example, the maximum of cohesive energy for Pt_9 in Figure 5 is explained by the conservation of the radius from Pt_8 (2.76 Å) while (9,20) possesses one atom and four MIDs more. A similar situation occurs for (6,5) with respect to (5,2). At the EHT level, when the consideration of the spherical density conflicts with these of the maximum number of MIDs, the most stable structure results from a compromise. This one is illustrated by the Pt_8 isomer (8,24), with 17 MIDs and a radius of 2.76 Å which is better than both (8,22) with a radius of 2.28 Å but only 16 MIDs, and (8,21) with 18 MIDs but a large radius (2.91 Å). Similarly, structure (9,20) with 21

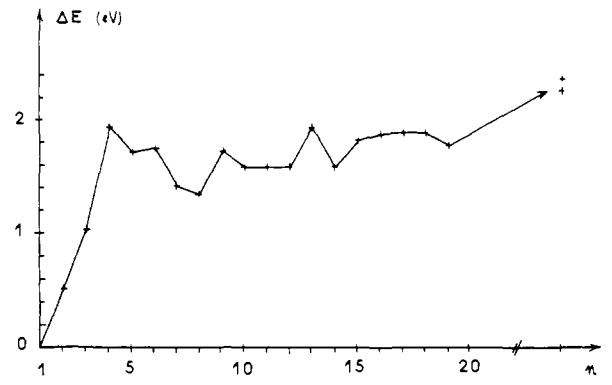

Figure 5. Plot of the variation of energy at the EHT–SO level for the reaction $Pt_{n-1} + Pt \rightarrow Pt_n$ vs. n.

MIDs and a radius of 2.76 Å is better than (9,23) with 18 MIDs and a radius of 2.40 Å. Structure (10,35) with 24 MIDs and a radius of 3.12 Å is more stable than (10,38) with 20 MIDs and a radius of 2.63 Å and than (10,31) with 25 MIDs and a radius 3.49 Å. Structure (11,1) with a radius of 3.20 Å and 29 MIDs is more stable than (11,15) with a radius of 2.63 Å and 25 MIDs. Structure (12,6) with a radius of 2.63 Å and 30 MIDs is more stable than (12,1) with 3.20 Å and 33 MIDs. At the SO level, all these highly spherical clusters, except Pt_4 (T_d) with an extra stabilization due to the first appearance of a large sp population as already discussed, have a small relative SO contribution (see Table III). It seems that for the molecules and atoms (s^0 and d^{10}) a spherical electronic distribution corresponds to a small SO contribution.

As atoms begin to coalesce in free space or, likewise, in a zeolite (assuming that metal–support interactions do not perturb the order of stability), we can expect that the $n = 4$, 6, 9, 13 Pt_n clusters will exist in relatively high concentration. The nonaggregation of these small clusters can only arise either from external stabilization by the surrounding environment (metal–support interactions, complexation by various ligands) or from entropy factors (dispersion of the fragments on the supporting material). Zeolites are, in both senses, favorable situations to observe clusters of small size.

Summarized in Table VI are the Fermi energy levels of the systems. The Fermi level is raised with the size of the cluster. For Pt_1, it is the highest d orbital; when the size of the clusters increases, the d band broadens out and the position of the Fermi level could only be pushed up to a high-energy value if the sp band did not exist. The existence of that band reduces the importance of the Fermi level shift. The calculated position of the Fermi level moves from −12.0 to −11.2 eV on going from Pt_2 to the bulk. Taking into account the spin–orbit coupling enlarges the band dispersion, and the resulting Fermi levels are pushed up to slightly higher values. The difference between the EHT and EHT + SO Fermi level is approximately 0.35 eV for a large range of clusters.

The net negative charge on the surface of the external layers of the infinite systems (Table VIII) results from the difference in the position of the Fermi level for the monolayers and the bulk.

Due to the evolution of the Fermi level with the size of the metallic aggregates, large systems may be assumed to be better electron donors than small ones. Furthermore, if a small system (cluster or infinite layer) is used as a model for a larger system (a surface), this model should be corrected in some way by adding electrons in order to put the Fermi level at its correct bulk position.

6. Conclusion

The present study gives the most stable isomers of the platinum clusters up to Pt_{13}. These clusters show a wide variety of shapes and no obvious pattern appears for the metallic growth up to this size.[23] Indeed, rarely, the most stable Pt_{n+1} cluster derives directly

(23) Sloane, N. J. A. *Sci. Am.* **1984**, *250*, 92.

from the most stable Pt_n cluster by addition of a single Pt atom to the unmodified compact Pt_n structure. This would imply the formation of an outgrowth which, except for the structure (8,21), cannot generate a structure with large spherical density. A significant reorganization is required to restore the compactness. In a similar way, the low-density surface of a crystal restructures relative to the crystal bulk. The number of MIDs is a good index number of the stability of the clusters of class A. Indeed, all its most stable clusters have the largest number of MIDs at the EHT level. This property is also true at the EHT-SO level except for the structures (11,1) and (12,1), which come after (11,2) and (12,2) while they have one MID less. These exceptions have been explained by the small geometrical constraints existing for bilayer clusters and by the sp populations.

When structures of class C are considered, the MID index number is only a helpful indication of the stability at the EHT level since some structures of class C have the largest cohesive energies without having the maximum number of MIDs. These structures have a large spherical density. Structures (8,24), (10,35), and (12,6) illustrate this point. As their SO contribution is weak, structures with the maximum number of MIDs ((8,21) from class C and (10,1) and (12,2) from class A) reappear as the most stable isomers at the EHT + SO level.

Since structures of class C are not suitable for an extension toward an infinite crystal and their cohesive energies are lower than for those of the fcc or hcp bulk, compounds of class A or B should prevail for the medium or large clusters. With such a growth, the mean number of MID per atom can converge to 6, the value for the bulk. For the small systems, the occurrence of some fragments of fcc or hcp type (Pt_3, Pt_4, Pt_5, Pt_6, Pt_{10}, Pt_{11}, Pt_{12}, and Pt_{13}) in the growth at the EHT + SO level is due more to their own compactness than to their classification as clusters of class A.

The EHT and EHT + SO methods are more selective than the simple Lennard-Jones interactions. For example, one Pt_{13} structure clearly emerges as the most stable within the EHT + SO framework while 987 structures are quasi-degenerate within a Lennard-Jones analysis.[3h]

The present results will be used to study the hydrogenation process of the Pt_n clusters.

Acknowledgment. This work has been supported by an ATP surface grant from the CNRS. We are pleased to thank Professor Fraissard for many discussions on the existence and the properties of small particles of platinum. We are grateful to Dr. Spanjaard for stimulating discussions on spin-orbit influence.

Registry No. Pt, 7440-06-4.

A Novel Isopiestic Measurement of Water Activity in Concentrated and Supersaturated Lithium Halide Solutions

C. B. Richardson* and C. A. Kurtz

Contribution from the Physics Department, University of Arkansas, Fayetteville, Arkansas 72701. *Received May 2, 1984*

Abstract: In a variation of the Stokes bithermal isopiestic method, single microscopic drops of lithium bromide and lithium iodide aqueous solution at room temperature are levitated electrodynamically in a closed chamber from which air is removed and to which is connected a vial of pure water at lower temperature. Water temperature is varied between -74 and +21 °C to measure concentrated and supersaturated solution water activity from 4.5×10^{-5} to 0.9. The results are compared with those of regular solution theory and the adsorption and stepped-hydration theories of Robinson and Stokes.

The isopiestic method for the determination of water activities in salt solutions is simple, precise, and general. Known amounts of nonvolatile solutes are placed in open containers in an isothermal enclosure into which water is introduced. At equilibrium the solution water activities are equal and the compositions are determined by weighing. With activities of reference solutions, e.g., NaCl, KCl, H_2SO_4, and $CaCl_2$, determined by vapor pressure and other measurements, the comparison method has yielded activities a_1 of hundreds of solutions over wide ranges of concentrations and temperatures.[1] With temperatures fixed to ±0.05 K or better, temperature differences between samples less than 10^{-4} K, and mass measurements precise to ±0.05%, the method yields composition ratios with a precision greater than 10^{-4} and ultimately, osmotic coefficients $\phi = -(N/\nu) \ln a_1$ with a precision greater than 10^{-3}. Here $N = [H_2O]/[X]$ is the solvent-solute and ν the ion-solute molar ratio.

A lower bound on a_1 is placed by the crystallization of the reference, e.g., $a_1 \geq 0.753$ for NaCl at 25 °C. In a variation on the method which avoids the lower bound, Stokes[2] replaced the solution reference with pure water at reduced temperature. He obtained good agreement with other measurements but did not push a_1 below 0.2889. A second lower bound is placed by crystallization of the unknown of course. Though many of the compounds listed in ref 1 have been measured to saturated solution, we know of no listings there for supersaturated solutions. Ionic solutions at the high concentrations of supersaturation may become ordered liquids for which water activity can serve as a probe.

We report here the results of an isopiestic study of lithium bromide and lithium iodide solutions by the Stokes method in which water activity is measured down to 4×10^{-5}. Our method differs in the handling of the sample. We have reduced its mass to 10^{-9} g, compared with the 1 g typical of isopiestic samples, have levitated it electrodynamically in a small sealed chamber from which air is removed, and have weighed it in situ and continuously with a noncontacting electrostatic balance.

With a microscopic spherical sample in a small chamber containing only water vapor, equilibrium is established much faster. More importantly, levitation of microscopic droplets allows supersaturation terminated only by homogeneous nucleation of crystallization.

We apply regular solution theory,[3] adsorption model theory,[4] and stepped-hydration model theory[5] to our results.

(1) Robinson, R. A.; Stokes, R. H., "Electrolyte Solutions"; Butterworths; London, 1959.
(2) Stokes, R. H. *J. Am. Chem. Soc.* **1947**, *69*, 1291.
(3) Pitzer, K. S. *Ber. Bunsenges. Phys. Chem.* **1981**, *85*, 952.
(4) Stokes, R. H.; Robinson, R. A. *J. Am. Chem. Soc.* **1948**, *70*, 1870.
(5) Stokes, R. H.; Robinson, R. A. *J. Soln. Chem.* **1973**, *2*, 173.

0002-7863/84/1506-6615$01.50/0